ADVANCED OPTICAL MATERIALS
www.advopticalmat.de

Novel Plasmonic Nanocavities for Optical Trapping-Assisted Biosensing Applications

Alemayehu Nana Koya, Joao Cunha, Tian-Long Guo, Andrea Toma, Denis Garoli, Tao Wang, Saulius Juodkazis, Dan Cojoc,* and Remo Proietti Zaccaria**

Plasmonic nanocavities have proved to confine electromagnetic fields into deep subwavelength volumes, implying their potentials for enhanced optical trapping and sensing of nanoparticles. In this review, the fundamentals and performances of various plasmonic nanocavity geometries are explored with specific emphasis on trapping and detection of small molecules and single nanoparticles. These applications capitalize on the local field intensity, which in turn depends on the size of plasmonic nanocavities. Indeed, properly designed structures provide significant local field intensity and deep trapping potential, leading to manipulation of nano-objects with low laser power. The relationship between optical trapping-induced resonance shift and potential energy of plasmonic nanocavity can be analytically expressed in terms of the intercavity field intensity. Within this framework, recent experimental works on trapping and sensing of single nanoparticles and small molecules with plasmonic nanotweezers are discussed. Furthermore, significant consideration is given to conjugation of optical tweezers with Raman spectroscopy, with the aim of developing innovative biosensors. These devices, which take the advantages of plasmonic nanocavities, will be capable of trapping and detecting nanoparticles at the single molecule level.

1. Introduction

Understanding the interaction of light with matter at the nanometer scale holds the key not only for improving our basic knowledge about the fundamental optical properties of nanomaterials but it is also crucial for their effective employment in a wide variety of applications such as sensing, energy harvesting, quantum information processing, and so on.[1–4] However, due to the intrinsic low optical response of small objects, there has been a clear trade-off between the size of a material and its response to light.[5] Recently, plasmonic nanostructures have emerged as leading platforms to enhance the weak optical signals of low dimensional materials including quantum dots (QDs),[6] small molecules,[7,8] and 2D monolayers.[9]

The plasmonic enhancement of linear and nonlinear optical processes capitalizes on the near- and far-field properties of metallic (e.g., gold and silver) nanostructures.[10] One of the defining features of plasmonic nanostructures is their potential to confine light into deep subwavelength volumes, which has opened a new door to trap and manipulate dielectric, metallic, and biological nano-objects.[11] Moreover, metallic nanostructures are characterized by their capability to amplify the intensity of optical fields by orders of magnitude. The enhancement of local field intensity is attributed to the resonance of plasmon polaritons arising from the coupling of external electromagnetic fields to the collective oscillations of the conduction electrons.[12] A small perturbation (or change in the refractive index) of the near field zone of plasmonic nanostructures leads to significant shift in the plasmon polariton resonance wavelength, which has important implications for surface-enhanced sensing and spectroscopic applications.[13,14] Thus, for the ad-hoc enhancement of optical

Dr. A. N. Koya, J. Cunha, Dr. T.-L. Guo, Dr. D. Cojoc, Prof. R. Proietti Zaccaria
Cixi Institute of Biomedical Engineering
Ningbo Institute of Materials Technology and Engineering
Chinese Academy of Sciences
Ningbo 315201, China
E-mail: alemayehu.koya@iit.it; cojoc@iom.cnr.it;
remo.proietti@nimte.ac.cn, remo.proietti@iit.it

The ORCID identification number(s) for the author(s) of this article can be found under https://doi.org/10.1002/adom.201901481.

DOI: 10.1002/adom.201901481

J. Cunha
University of Chinese Academy of Sciences
Beijing 100049, China

Dr. A. N. Koya, Dr. A. Toma, Dr. D. Garoli, Prof. R. Proietti Zaccaria
Istituto Italiano di Tecnologia
via Morego 30, 16163 Genova, Italy

Prof. T. Wang
School of Electronics and Information
Hangzhou Dianzi University
Hangzhou 310018, China

Prof. S. Juodkazis
Nanotechnology Facility
Center for Micro-Photonics
Swinburne University of Technology
Hawthorn, VIC 3122, Australia

Dr. D. Cojoc
CNR-IOM
Trieste 34149, Italy

fields, it is crucial to design and engineer plasmonic nanostructures with tunable resonance features and versatile geometries, which may provide several degrees of freedom for an efficient functionalization of the nanostructures according to the desired application.

Among several geometries, plasmonic nanocavities with subdiffraction volumes are capable of confining electromagnetic fields into ultrasmall volumes resulting in giant local field enhancement. These kinds of deep subwavelength nanocavities can be realized either by coupling two nanostructures with sub-nanometer interstructure gap or by engraving nanoholes in thin metallic films. For example, the particle-on-mirror (PoM) cavity is formed by placing a nanoparticle just above a thin metallic layer thus forming a dimer-like structure with a plasmonic hot spot centered between the nanoparticle and the substrate. PoM nanocavities, which can support multiple resonances, exhibit deep subdiffraction mode volumes below $10^{-7}(\lambda/n)^3$ (where λ is the wavelength and n is the refractive index of the cavity).[15–19] Similarly, dimer nanocavities are realized by bringing two metallic nanostructures into close proximity, resulting in the coupling of their electromagnetic fields which gives rise to an intensely confined hotspots localized inside the gap.[20] Finally, aperture nanocavities, which can take shapes such as bowtie, rectangular or circular, are formed by engraving nanoholes in thin metallic films.[21–26] These geometries have proved to be powerful platforms for such purposes as trapping and manipulation of nano-objects,[27,28] sensing applications,[29] enhancement of Raman signal of small molecules,[30] and realization of strong light–matter interactions.[31–33]

Within this context, the present review explores the fundamentals and functionalities of various plasmonic nanocavity layouts targeting application in biosensing through optical trapping and surface-enhanced Raman spectroscopy (SERS). In particular, the review aims at exploiting the potentials of plasmonic nanocavities for developing optical trapping-assisted SERS sensing devices. These devices mainly rely on the local field intensity, which in turn depends on the cavity gap size. Thus, examining the ultimate limits of plasmonic enhancements in both classical and quantum regimes of the cavity sizes is important. To this end, we discuss the optical responses of plasmonic nanocavities and their functionalities at sub-nanometer cavity size where the nonlocal and quantum mechanical effects cannot be neglected.[34,35] The review is organized as follows: a description of the fundamental physics and design parameters of plasmonic nanocavities for optimal optical responses is reported after the Introduction. In third section, the basic principles of near-field optical trapping in plasmonic nanocavities are discussed. The fourth section stresses on optical trapping-induced resonance shift of plasmonic nanocavities with particular focus on developing analytical expressions for relating optical trapping potential (U) with trapping-induced resonance shift ($\Delta\omega$) of plasmonic nanocavities. In section fifth, biosensing of single nanoparticles and small molecules with plasmonic nanoaperture tweezers are investigated. Finally, this work is concluded by analyzing the possibility of developing plasmonic optical trapping-assisted Raman sensing platforms from both theoretical and practical perspectives.

Alemayehu Nana Koya is a postdoctoral researcher at the Italian Institute of Technology (IIT), Genova, Italy. He received his Ph.D. in Optics from Changchun University of Science and Technology, China, in 2017. Prior to joining IIT, he had been working for the Chinese Academy of Sciences as a postdoctoral researcher and visiting scientist. His research focuses on exploring the fundamentals and functionalities of plasmonic and photonic crystal nanocavities. Currently, he is working on exploiting the potentials of hybrid nanocavities for enhancing optical trapping, biosensing, and nanolasing applications.

Remo Proietti Zaccaria is a group leader at the Multiphysics Laboratory at the Italian Institute of Technology and a professor at the Cixi Institute of Biomedical Engineering, Ningbo Institute of Materials Technology and Engineering, Chinese Academy of Sciences. His work mainly aims at modeling and experimentally validating complex systems at the micro/nanoscale with strong emphasis on the final device. In particular, his research themes focus on the integration of different physics (i.e., interdisciplinary) such as photonics, heat diffusion, electric charge/mass diffusion, and mechanical deformation toward the development of innovative devices for energy manipulation (harvesting and storage).

2. Optical Properties of Plasmonic Nanocavities

The optical responses of plasmonic nanocavities strongly depend on their geometrical design as well as irradiation field parameters such as polarization and excitation wavelength.[36,37] In particular, the electromagnetic properties of nanocavities are extremely sensitive to morphological fluctuations and subtle changes in the dielectric properties of the cavity contents.[19] Thus, parameters pertaining to the nanocavity design, such as nanostructure configuration[30] and cavity gap size,[38] play important roles in modifying both the near-field intensity and far-field radiation of the proposed architectures. Here, we discuss optical responses of plasmonic nanocavities with different geometries in both classical and quantum regimes.

In dimer nanocavities, both the near- and far-field responses strongly depend on the interparticle gap. When two metallic nanostructures are brought into close proximity where the interparticle gap is smaller than the nanoparticle size, the

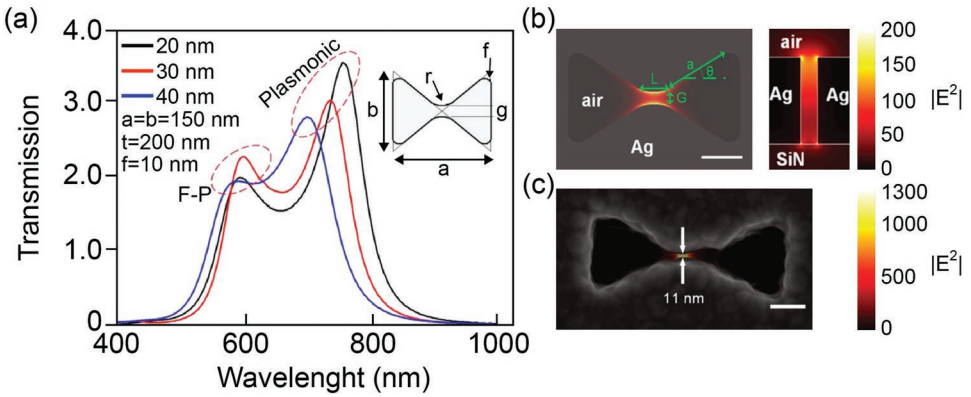

Figure 1. Optical properties of bowtie aperture nanocavities. a) Transmission efficiency through bowtie apertures defined in 200 nm thick silver film as a function of cavity gap distances of g = 20, 30, and 40 nm for fixed aperture length a = 150 nm, width b = 150 nm, ridge radius r = 30 nm, and corner radius f = 10 nm. Reproduced with permission.[36] Copyright 2016, Springer Nature. b) Schematic illustration and near-field profiles of a bowtie aperture fabricated in 100 nm thick silver film with cavity gap G = 30 nm, gap length L = 82 nm, arm length a = 150 nm, and arm angle θ = 30°. The side view of the fundamental gap mode field profile shows the Fabry–Perot like resonance with one node inside. c) SEM image of a bowtie aperture with G = 11 nm, overlapped with field intensity enhancement profiles at its resonance wavelength. This aperture can have an intensity enhancement as high as 1300. The scale bars are all 100 nm. Reproduced with permission.[22] Copyright 2016, AIP Publishing.

optical responses of the system clearly displays the formation of hybridized modes, enhanced near-field intensity, and redshifted far-field spectrum.[39–41] The plasmonic coupling of metallic nanodimers gives rise to an intense confinement of electromagnetic fields in the gap region,[42] which has significant relevance for surface-based sensing applications.[14]

On the other hand, aperture nanocavities are realized on metallic films and support two types of resonant modes, namely Fabry–Perot (F–P) and plasmonic modes.[21,22] The F–P resonance is sensitive to the thickness of the metallic film whereas the plasmonic mode mainly depends on the geometric parameters of the aperture. These two distinct modes are highlighted in **Figure 1**a that shows simulated transmission spectrum of a bowtie aperture defined in a 200 nm thick silver film on top of a fused silica substrate.[36] The intensities and resonance wavelengths of both modes strongly depend on the cavity gap size g that is defined in terms of aperture parameters: $g = 2r\left(\frac{1}{a}\sqrt{a^2 - b^2} - 1\right)$, where a is the length, b width, and r ridge radius of the aperture, as illustrated in the inset of Figure 1a. Thus, the cavity mode can be easily tuned by changing one of the nanoaperture parameters. Similarly, the resonantly calculated near-field profiles shown in Figure 1b,c reveal that bowtie apertures have the unique capability of confining electromagnetic fields into ultrasmall mode volumes with giant field intensity enhancements.[21,22] Kim et al. have experimentally demonstrated that a 3D plasmonic bowtie nanoaperture with cavity gap of g = 4 nm can squeeze photon into a point-like 3D space with a modal volume of $1.3 \times 10^{-7}\ \lambda^3$ ($V \approx 4 \times 10 \times 10\ \text{nm}^3$) and local field intensity enhancement of about five orders of magnitude ($|\mathbf{E}|^2 \sim 4 \times 10^5$).[21] Hence, bowtie nanoapertures with high collection cross-section and transmission as well as strong mode confinement under transversal polarization are very good premise for optical trapping.[27,28]

Similarly to the bowtie aperture in design, double nanohole (DNH) cavities present versatile geometries with intriguing optical properties. DNH apertures are designed in different ways and fabricated by focused ion beam milling into a thin plasmonic film (**Figure 2**a,b). Gordon and co-workers have theoretically proposed and experimentally demonstrated that, like bowtie apertures, double nanohole apertures can exhibit various modes depending on the cavity design.[43–46] For example, a slope of metallic wedges in appropriately designed DNH apertures leads to excitation of wedge plasmon polariton (WPP), which couples to the gap surface plasmon (GSP) resonance in addition to the well-known zeroth order Fabry–Perot mode (FP0).[45,46] These modes are evident from the calculated transmission spectra shown in Figure 2c for various nanohole shapes. The WPP peak appears at λ = 678 nm for conical nanoholes with top and bottom radii of R_t = 70 nm and R_b = 56 nm, respectively. When the cusp profiles are estimated by cylindrical geometries, the WPP can be hardly detected. However, the FP0 peak appears for both conical and cylindrical geometries at longer wavelength ($\lambda \approx$ 1000 nm). The nature of various modes emerged in the transmission spectra of the conical and cylindrical geometries are further illustrated in resonantly calculated local field intensities for three wedge profiles shown in Figure 2d–f. Based on the local field intensity profiles of both geometries, one can note that conical aperture geometries provide higher field intensities than cylindrical ones. Similar local field features are observed in slanted bowtie aperture nanocavities reported by Kim et al.[21] These results suggest the possibility of using aperture nanocavities for optical trapping, sensing, and Raman spectroscopy.[25,26,29,45,46]

An important aspect to be considered when dealing with optical nanocavities is that they are inherently dissipative, a situation that can be quantified by key parameters such as the quality factor, Q-factor, and the effective mode volume, V_{eff}. These two quantities describe the relative energy loss per cycle and the spatial confinement of light in the cavity, respectively.[47] Cavities with high Q values and small mode volumes provide enhanced light–matter interaction and thus are of both fundamental and technological interest.[48] The canonical definition of the effective mode volume of optical cavities is given as[47,48]

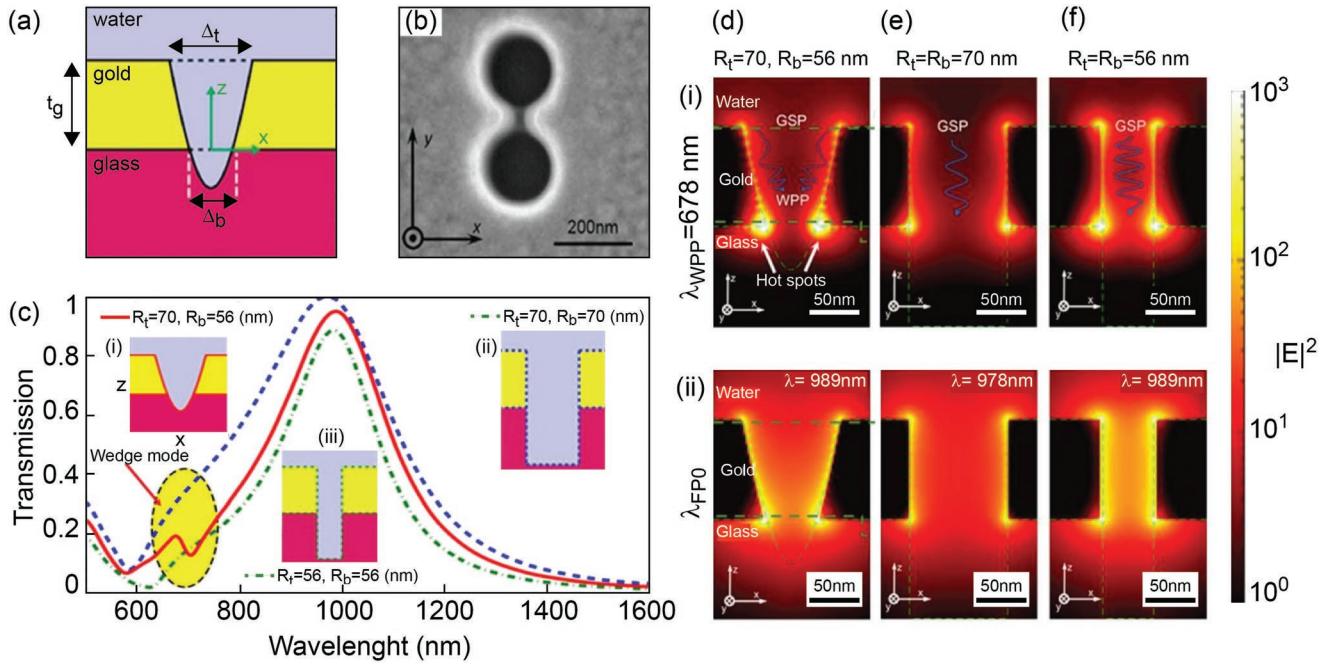

Figure 2. Optical properties of double nanohole (DNH) aperture nanocavities. a) Schematic of *x*–*z* cross-section of the DNH aperture milled in gold layer with top (Δ_t) and bottom Δ_b) tip separations defined by respective hole radii R_t and R_b. b) SEM image of the DNH fabricated by milling focused ion beam into a gold film with thickness t_g = 100 nm. c) Comparison of the transmission spectra, calculated for the DNH structures estimated by conical (solid curve) and cylindrical holes (dashes and dashes-dots). The insets show the *x*–*z* cross-sections of the three estimated profiles. The corresponding mode profiles calculated at various resonant modes are shown in column d) for conical double nanoholes and in e,f) for cylindrical double nanoholes with different radii. The field profiles shown in rows (i) and (ii) are calculated at the wedge plasmon polariton (WPP) and Fabry–Perot modes (FP0), respectively. The vertical bar scales display enhancement of the mode intensities $|E|^2$. Reproduced with permission.[46] Copyright 2017, ACS Publications.

$$V_{\text{eff}} = \int_V \frac{\varepsilon(\mathbf{r})\left|\mathbf{f}_c(\mathbf{r})\right|^2}{\varepsilon(\mathbf{r}_c)\left|\mathbf{f}_c(\mathbf{r}_c)\right|^2}\,\mathrm{d}\mathbf{r} \tag{1}$$

where $\varepsilon(\mathbf{r})$ is the relative permittivity, $\mathbf{f}_c(\mathbf{r})$ represents the cavity mode and $\mathbf{r}_c$ is the antinode position. This expression is based on the assumption that the mode is localized in space. However, in reality, all optical cavities have finite leakage, which leads to modes that diverge in space. Consequently, the mode volume given in Equation (1) diverges exponentially. In particular, when dealing with low Q cavities or plasmonic nanostructures this problem is much more severe. Moreover, for structures containing lossy materials such as metals, the integrand of Equation (1) will become negative when the dielectric constants $\varepsilon < 0$.[49] Thus, a generalized expression for effective mode volume is needed. To meet this demand, Hughes and co-workers developed a generalized expression for leaky optical cavities[47,48]

$$\frac{1}{V_{\text{eff}}^{Q}} = \text{Re}\left\{\frac{1}{v_Q}\right\}, \qquad v_Q = \frac{\langle\langle \tilde{\mathbf{f}}_c \,|\, \tilde{\mathbf{f}}_c \rangle\rangle}{\varepsilon(\mathbf{r}_c)\tilde{\mathbf{f}}_c^2(\mathbf{r}_c)} \tag{2}$$

where the generalized mode volume v_Q is complex in general and $\tilde{\mathbf{f}}_c^2(\mathbf{r}_c) = \tilde{\mathbf{f}}_c(\mathbf{r}_c)\cdot\tilde{\mathbf{f}}_c(\mathbf{r}_c)$. This prescription is believed to provide a direct and unambiguous way of calculating the effective mode volume for arbitrary cavities. Similarly, Maier developed a slightly different formulation for lossy metals[50–52]

$$V_{\text{eff}}(\mathbf{r}_0) = \frac{\int u_E(\mathbf{r})\,\mathrm{d}\mathbf{r}}{u_E(\mathbf{r}_0)} \tag{3}$$

where $\mathbf{r}_0$ is the spatial position of the mode of interest, and $u_E(\mathbf{r})$ is the electromagnetic field energy density at the spatial position r, which is expressed as[52]

$$u_E = \frac{\varepsilon_0}{2}\left(\varepsilon_1 + \frac{2\omega\varepsilon_2}{\gamma}\right)|\mathbf{E}|^2 \tag{4}$$

where $\varepsilon(\omega) = \varepsilon_1(\omega) + i\varepsilon_2(\omega)$ is the complex dielectric function of materials according to the Drude model with damping γ and $|\mathbf{E}|$ is the electric field amplitude.

Generally, plasmonic nanocavities can achieve a much smaller mode volume than standard optical cavities being them capable of confining the electromagnetic energy far beyond the diffraction limit.[53] However, plasmonic nanocavities are limited by high intrinsic losses of metals, leading to low quality factor Q. As stated above, the Q-factor is related to the dissipation rate of photons confined in the cavity and defined as $Q = \omega_0/\Delta\omega$ (where ω_0 is the resonant frequency and $\Delta\omega$ is resonant linewidth).[54] Generally, nonlossy materials have high Q-factor whereas lossy materials, such as gold and silver, have low Q-factor. High Q-factor is often needed for realization of optical processes such as enhanced spontaneous emission, optical nonlinearity, strong coupling, and optomechanic effects.[55,56] To increase the Q-factor, plasmonic nanocavities are often hybridized with high Q-factor structures like dielectric cavities and photonic crystals.[57] However, it is important to underline that Q-factor of a nanocavity is not the key parameter for applications such as sensing and SERS.[58]

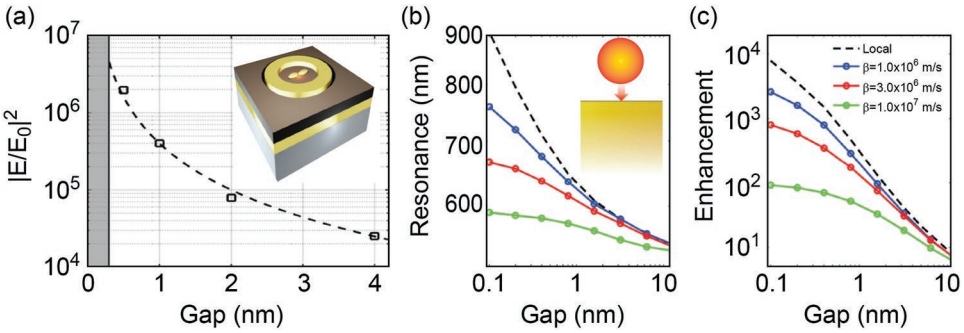

Figure 3. a) Numerically calculated results (squares) of local intensity enhancement scaling with the gap separation of a prolate spheroid dimer (shown in the inset). The theoretical fit (dotted line) has an inverse squared dependence, since the field alone should scale as the inverse of the gap size. The left vertical grey region shows the onset of significant tunneling effect in vacuum at 0.3 nm gap separation. Reproduced with permission.[59] Copyright 2018, ACS Publications. b,c), respectively, represent the far-field and near-field optical behaviors of a particle-on-film nanocavity, assuming local model and nonlocal models with various values of the nonlocality parameter, as a function of the cavity gap. Calculations refer to a gold nanosphere of radius $r = 30$ nm on a film 300 nm thick. Reproduced with permission.[60] Copyright 2012, AAAS.

2.1. Nonlocal Effect

One of the most remarkable phenomena associated with plasmonic nanostructures at optical wavelengths is field enhancement. And most plasmon-based applications mainly rely on the local field intensity of the metallic nanostructures. From a classical point of view, the local field enhancement factor (EF) in the cavity is obtained from integral volume average of $|\mathbf{E}/\mathbf{E}_0|^2$[16,38]

$$EF = \frac{\iiint |\mathbf{E}/\mathbf{E}_0|^2 \mathrm{d}V}{V} \tag{5}$$

where $\mathbf{E}$ is the local maximum electric field, $\mathbf{E}_0$ is the impinging amplitude of the source electric field, and V is the volume. For the incident amplitude $\mathbf{E}_0 = 1$ V m^{-1}, the local field intensity of plasmonic nanocavity is often expressed as $|\mathbf{E}|^2$. As it can be seen from **Figure 3**a, the local field enhancement factor calculated in the cavity of a prolate spheroid dimer shows monotonous increment as the dimer gap decreases, showing an inverse squared dependence.[59] However, for a gap separation below 1 nm (see the grey region in Figure 3a), nonlocal effects arise and limit the extraordinary field enhancement.[34,35]

The conventional classical Drude model of local dielectric function of metals is expressed as

$$\varepsilon(\omega) = 1 - \frac{\omega_p^2}{\omega^2 + i\gamma\omega} \tag{6}$$

where ω_p is the bulk plasma frequency and γ is damping coefficient. However, the local model is insufficient to describe the optical responses of metallic nanostructures whose critical dimensions are on the order of a few nanometers. Thus, more appropriate description that considers subatomic interactions and electron–electron repulsion is needed. Recently, a hydrodynamic description that takes the electron pressure into account has been reported.[34,60] Accordingly, the pressure-gradient supplemented motion equation for an electron in a time harmonic electric field $\mathbf{E}$ is written as[34]

$$m\frac{\mathrm{d}\mathbf{v}}{\mathrm{d}t} = -e\mathbf{E} - m\gamma\mathbf{v} - \frac{m\beta^2}{n_0}\nabla n_1 \tag{7}$$

where $\mathbf{v}$ is the electron velocity, γ is the damping term, e is the charge of an electron, β is a parameter proportional to the Fermi velocity $\mathbf{v}_F$, and n_1 is the linear perturbation of the electron density which is given as

$$\nabla n_1 = \frac{n_0}{i\omega}\nabla\nabla\mathbf{v} = \frac{n_0}{i\omega}\nabla^2\cdot\mathbf{v} \tag{8}$$

By inserting Equation (8) into Equation (7) and solving in Fourier space to determine the induced polarization, one arrives at

$$\varepsilon(\omega,\mathbf{k}) = 1 - \frac{\omega_p^2}{\omega(\omega+i\gamma) - \beta^2\mathbf{k}^2} \tag{9}$$

Equation (9) is often termed as hydrodynamic Drude dielectric function and it explicitly depends not only on the frequency ω but also on the wave vector $\mathbf{k}$. The extent of nonlocality of the dielectric function is controlled by β.[34,60]

While the above analytical approach can provide intuitive information about the nonlocal effects, it is important to validate these expressions with simulations in order to quantitatively analyze the resonance pattern and local field enhancement at the sub-nanometer scale. The nonlocal effect on the near- and far-field responses of plasmonic nanocavity made of particle-on-mirror geometry is displayed in Figure 3b,c. Both the plasmon resonance peak positions and enhancement factors are significantly affected by the nonlocal effect.[60] In the absence of nonlocal effects ($\beta = 0$), the peak scattering wavelength is extreme and the field enhancement grows to enormous values as the cavity separation decreases from 10 to 0.1 nm. For the local model of the dielectric function, the plasmon resonance wavelength is pushed to nearly $\lambda = 900$ nm, corresponding to a peak local field enhancement of $|\mathbf{E}|^2 \sim 10^4$. For $\beta \neq 0$, the impact of the nonlocal electronic response is decisive, causing the peak resonance wavelength to occur at values much lower than that predicted by the local model. In particular, by assuming $\beta = 1.0 \times 10^7$ m s^{-1}, the resonance peak is about $\lambda = 300$ nm blue shifted with respect to the local model results and local field enhancement is reduced to 10^2, which is about two orders of magnitude

smaller than that achieved by the local model for 0.1 nm gap size.

On the other hand, a number of experimental and theoretical reports claim the absence of nonlocal effects in plasmonic sub-nanometer gap structures due to the breakdown of the local density approximation. In their seminal report on the interaction between two metallic nanowires with separations down to the angstrom range, Teperik et al. demonstrated full equivalency between the results obtained from the quantum time-dependent density functional theory and the results from the classical Drude model.[61] Similarly, self-assembled monolayers (SAMs) have been used as plasmonic rulers to measure the nonlocal influence on the resonance shift of Au nanoparticle–metal film structures. Using SAMs, Hajisalem et al. have studied the influence of the surface roughness on plasmonic rulers in the nonlocal regime.[62] They showed that the resonance shift is larger for ultraflat films without any saturation from nonlocal effect that was previously reported for the spacer ranging from 0.7 to 1.6 nm. Doyle et al. also carried out extensive study on the refractive index of self-assembled sub-nanometer gap plasmonic metasurfaces at visible and near-IR wavelengths.[63] They experimentally demonstrated that the optical responses of the metasurfaces agree well with the classical local model, with a minor nonlocal effects as the interparticle gaps approach atomic lattice scale ≈0.45 nm.

3. Optical Trapping in Plasmonic Nanocavities

Since Ashkin's first demonstration of acceleration of particles by radiation pressure,[64] the research on optical manipulation of micro/nanoobjects has shown a tremendous progress. Conventional optical tweezers use high numerical aperture (NA) lenses to focus laser beams, thus providing the required optical force for trapping and manipulation of micro and nanosized particles. However, as a result of the diffraction limit of light, the optical lenses cannot focus laser beams to spot sizes smaller than roughly half the light wavelength making it impossible to extend the optical trapping down to the single-molecule scale.[65] Moreover, trapping nanosized objects with the conventional optical tweezers requires high laser intensity, which might cause an optical damage to heat-sensitive objects such as biospecimens.[27] However, with the advancement of the nanophotonics, this limitation has been overcame by employing plasmonic nanostructures that can confine and enhance electromagnetic fields within ultrasmall volumes well beyond the diffraction limit.[66,67] These tightly confined optical near-fields have intriguing implications for trapping and manipulation of small molecules and single nanoparticles.[25–28] After introducing the basic principles of optical trapping, thus, the unique potentialities of plasmonic nanocavities for trapping nanosized objects with low field intensities will be discussed.

3.1. Principles of Optical Trapping

Conventional optical trapping occurs when a laser beam is tightly focused through a high NA lens onto a particle that is placed near the focus. The particle experiences an optical force due to change in the momentum of the light interacting with the particle.[68,69] The nature of the optical forces is investigated for different trapping regimes, which are determined by the size of the trapping object. When the size a of the trapped object is much smaller than the wavelength λ of impinging laser ($a \ll \lambda$), the conditions for Rayleigh scattering regime are satisfied.[70] In this regime, the incident electromagnetic field is regarded as uniformly distributed around the particle, and the polarizability α can be computed using electrostatic approximation[71]

$$\alpha = \alpha' + i\alpha'' = 3V \frac{\varepsilon_p - \varepsilon_m}{\varepsilon_p + 2\varepsilon_m} \tag{10}$$

where $\varepsilon_p = \varepsilon_1 + i\varepsilon_2$ and $\varepsilon_m = n_m^2$ are the dielectric constants of the particle and the surrounding medium, respectively, whereas $V \propto a^3$ is the volume of the Rayleigh particle. The net optical force acting on the nanoparticle has three components: absorption F_{abs}, scattering F_{scat}, and gradient F_{grad} forces, respectively expressed as[72,73]

$$F_{abs} = \frac{n_m \langle \mathbf{P} \rangle C_{abs}}{c} \tag{11}$$

$$F_{scat} = \frac{n_m \langle \mathbf{P} \rangle C_{scat}}{c} \tag{12}$$

$$F_{grad} = \frac{|\alpha|}{2} \nabla \langle \mathbf{E}^2 \rangle \tag{13}$$

where $\mathbf{P}$ is the Poynting vector, $C_{abs} = k(\alpha'')$ and $C_{scat} = k^4|\alpha|^2/4\pi$ represent the absorption and scattering cross-sections of the Rayleigh particle, $k = 2\pi n_m/\lambda$, wave number of the surrounding medium, c speed of light in vacuum, and $\langle \mathbf{E}^2 \rangle$ is intensity of light.

The absorption and scattering are repulsive forces that push the particle away in the direction of beam propagation, whereas the gradient force attracts the particle in the direction of the spatial gradient of the light intensity.[71] To achieve nanoparticle trapping, the gradient force must exceed the sum of the absorption and scattering forces. From the gradient formula one can note that a strong axial gradient of intensity, which is obtained by tightly focusing the trapping beam, is crucial to produce a net backward axial force component. Moreover, as it can be seen from the equations, all the components of the optical forces depend on the polarizability α of the Rayleigh particle. Dielectric particles such as silica and beads have positive α ($\varepsilon_p > \varepsilon_m$), therefore, they will be pulled toward the maximum optical intensity of a Gaussian beam with transverse (TEM_{00}) mode.[74] Particles like phospholipid-shelled gas microbubbles can be trapped using a Laguerre–Gaussian (LG_{01}) beam, with a doughnut like intensity profile that confines the particle within the doughnut.[75,76] As implied in Equations (12) and (13), the scattering force F_{scat} scales with α^2 whereas the gradient force F_{grad} scales with α. Thus, the necessary axial trapping condition $F_{grad} >> F_{scat}$ becomes very favorable for nanosized dielectric particles.

However, a net balance of forces is only a necessary but not sufficient condition for Rayleigh trapping. As the nanoparticle size decreases, its polarizability becomes smaller, thus we need to increase the laser intensity. On the other hand, maximizing the gradient force by decreasing the particle size causes

instability and the particle undergoes Brownian motion.[77–79] For a stable trapping of a nanoparticle, thus, the trapping potential created by radiation must overcome the thermal energy k_BT (where k_B is the Boltzman constant and T is the absolute temperature).[71] Accordingly, an additional sufficient trapping condition implies the Boltzmann factor $\exp(-U/k_BT) \ll 1$, where $U = n_b \frac{\alpha}{2} |\mathbf{E}|^2$ is the potential of the gradient force with n_b the refractive index of the surrounding medium.[64,69] This requirement leads to the fact that if the trapping potential significantly exceeds the thermal kinetic energy, the particle is less probable to escape the potential well due to the Brownian motion. By setting $U/k_BT \geq 10$ as threshold criterion, and using 1.5 W laser power focused by a lens with NA of 1.25 to the limiting spot diameter of 0.58 µm, Ashkin et al. experimentally demonstrated trapping of silica beads of 26 nm diameter.[69] They also predicted the minimum theoretical particle sizes that can be trapped under these conditions (19 nm for silica and 14 nm for polystyrene (PS) latex). Concurrently, Oddershede and co-workers demonstrated stable trapping of metallic nanoparticles with diameters down to 20 nm.[72]

3.2. Plasmonic Optical Tweezers (POTs)

It is well known that the polarizability of trapping particle and the intensity of the laser power are the main parameters of optical tweezers. However, as the object size decreases, its polarizability also decreases, which makes it more challenging to obtain stable trapping.[80] Consequently, for stable trapping of nanosized objects and small molecules with conventional optical tweezers, high laser intensity, in the range of 10^{11}–10^{12} W m^{-2}, is required.[27] Such a high level intensity might cause damage not only to heat-sensitive objects such as biological specimens but also to metallic particles that have high absorption.[81] To overcome this problem, and to manipulate nanometer-sized objects beyond the diffraction limit, a novel optical tweezer that capitalizes on the local field intensity of metallic nanostructures has been introduced.[11,67] In such optical trapping approach, commonly referred as POT,[73] the interaction of incident light with the nanostructures creates large evanescent fields, resulting in subwavelength concentration of light within subwavelength regions.[82,83] In other words, plasmonic nanostructures function as nanolenses that are capable of concentrating light well beyond those of high NA lenses used in the conventional optical tweezers.[67]

Generally, POTs have several advantages over conventional optical tweezers. First of all, the high intensity source needed to achieve stable trapping of small nanoparticles is reduced by the field enhancement effect of plasmonic nanostructures.[71,84,85] In addition, the motion of trapped nanoparticles can be tightly bound to a space much smaller than the diffraction limit of light (**Figure 4**). Finally, plasmonic optical tweezers have the potentials to be combined with other optoelectronic devices which would lead to novel applications.[86–88] However, because of photothermal effects, plasmonic trapping is limited to specific object sizes, which are estimated to be ≥100 nm.[67,71,80] These observations imply the existence of a clear trade-off between the size of a particle to be trapped, its spatial confinement, and the intensities required to trap the nanoparticle. To overcome this limitation and to extend the trapping efficiency of POTs, an alternative strategy, the so called self-induced back-action (SIBA) trapping, inspired by the concept of opto-mechanics, has been adopted.[5,80,89]

3.3. Self-Induced Back-Action Optical Trapping

In SIBA optical trapping, the trapped object strongly influences the strength of local field enhancement and thereby plays an active role in the trapping process through self-induced back-action effect.[90,92–94] In this strategy, the cavity resonance is modulated by the changes in the particle position, resulting in a dynamic optical trapping whose long-term stability requires much lower average intensities compared with a static potential.[80] Following this approach, it was possible to trap sub-100 nm objects as well as individual biomolecules by using an average local field intensity orders of magnitude weaker than from conventional optical tweezers.[27,80] These moderate field intensities are particularly important for trapping small particles such as dielectric nanoparticles, proteins, and viruses, which have small polarizabilities and sensitive to the local heating effect.[24] The SIBA trapping in plasmonic nanocavities relies on the high sensitive shift of the plasmon resonance induced by the presence of specimen.[24] As the trapping object enters the close vicinity of the nanocavity, the effective local refractive index of the plasmonic nanocavities increases inducing redshift of the cavity resonance and consequently change of the far-field and local field intensities.[24] To maximize the SIBA effect the nanocavity should be designed in such a way that its far-field resonance spectrum and local field intensity would significantly depend on the position of trapping object.[27] This can be achieved by designing a nanocavity

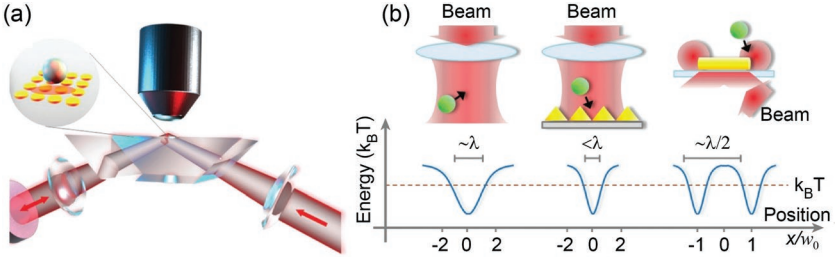

Figure 4. Plasmonic optical tweezers. a) Schematic of the Kretschmann configuration. The laser beam is guided through a prism. Evanescent optical waves are excited at the interface between a high (glass prism) and a low (water) refractive-index medium; the beam is incident at the total-internal-reflection angle. Plasmonic structures such as nanopillars, nanoholes, nanopyramids, etc. (inset) are used to create high local fields confined in a subdiffraction volume and able to efficiently trap nanoparticles. A microscope objective, atop, is used to image the sample. b) Comparison of designs and performances for conventional (left) and plasmonic optical tweezers (center, right). Notice how POTs are exploited to create more localized and intense fields than their conventional OTs counterpart. In POTs the linear size of the trap can break the diffraction limit, with specific designs (right) offering dramatic confinement. Note that scales of reference are approximate. Depths of the potential can change based on size and properties of the nanoparticles. Reproduced with permission.[142] Copyright 2018, Wiley-VCH.

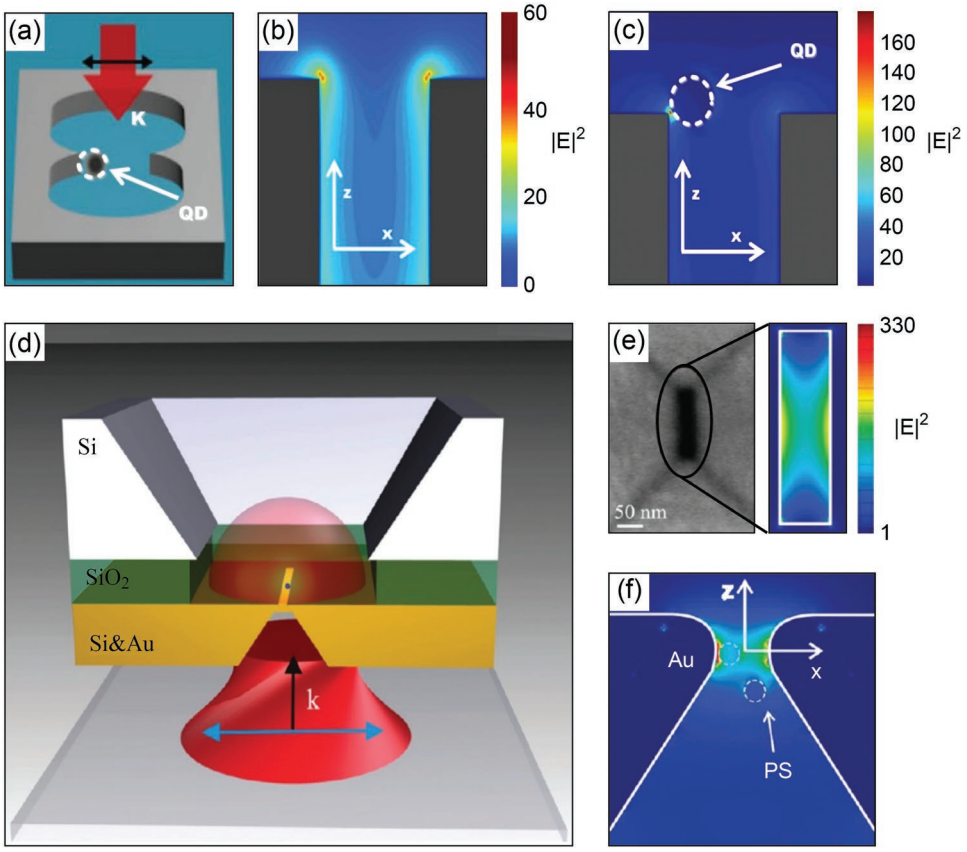

Figure 5. SIBA Optical trapping in plasmonic nanocavities. a) Schematic of SIBA trapping of 8 nm sized quantum dot (QD) in a double nanohole silver aperture. The nanocavity is made of two elliptical shaped nanoholes connected by 20 nm slot. b,c), respectively, represent the local field intensity $|E|^2$ of the aperture cavity in the absence and presence of the quantum dot at one of the nanocavity tips. Gray areas indicate the silver patch structures. Reproduced with permission.[94] Copyright 2018, Chinese Laser Press. d) Schematic drawing of the trapping setup for a Fabry–Perot nanopore cavity (40 × 170 nm^2) in a freestanding silicon membrane coated with a 100 nm thick gold layer. The incident light is focused at the cavity, and the transmitted light is detected at the other side of the chip. A single polystyrene (PS) bead (blue) is trapped inside the nanopore. e) SEM image of the nanopore and FDTD simulated field distribution inside the pore at its resonance (top view). f) FDTD simulated field distribution for the double bead trapping (side view): The first PS bead is trapped by the hot spot at one of the nanopore edges, while the second one is approaching. The origin of the coordinate system is at the center of the nanopore where the gap size is the smallest. Reproduced with permission.[24] Copyright 2011, ACS Publications.

slightly blue detuned in absence of the trapped object. The red shift of the cavity resonance induced by the presence of the trapped object sets the nanostructure on resonance, increasing optical near-field intensity.[24,94]

To date a number of theoretical and experimental works on near-field optical trapping involving SIBA approach have been reported.[5,11,24,27,80,89,94] The theoretical work reported by Zhang et al. reveals that the trapping of 8 nm sized single QD in 20 nm gap silver nanocavity (**Figure 5**a) results in significant variation in the local field intensity.[94] In absence of the quantum dot, the local field intensity shows uniform distribution around the cavity region (Figure 5b). However, when the QD is placed near to one of the cavity tips, the hot spots around the quantum dot shows higher intensity compared with other regions of the nanocavity (Figure 5c). This reveals that the self-induced back action of quantum dot plays an active role in modifying the local field intensity of the nanosystem. Similarly, Chen et. al. successfully demonstrated SIBA trapping of 22 nm PS beads in a rectangular-shaped (40 × 170 nm^2) gold nanoaperture (Figure 5d). Simulation results of the local field distribution shown in Figure 5e,f reveal that the intensity of the cavity hot spot is further enhanced by the presence of the PS beads.[24] These observations imply that the local field intensity of coupled particle–cavity nanosystem depends not only on the optical response of the bare nanocavity but also on the trapped particle. In this respect, the recent advancements in the quantity and quality of theoretical and experimental reports based on this approach make the SIBA effect a very much discussed topic, possibly suggesting SIBA as the future for the near-field optical trapping.

3.4. Parameters of Near-Field Optical Trapping

For a clear understanding of the near-field optical trapping, quantitative expressions of physical quantities such as optical forces and trapping potentials have to be properly defined. In their seminal work of nanoscale optical tweezers, Novonty et al. formulated theoretical description of near-field optical trapping based on highly enhanced electric field close to a metal tip.[66]

The total optical force acting on a nanoparticle placed in near-field zone is determined by the Maxwell stress tensor (MST) formalism. Here, the time-averaged optical force $\langle \mathbf{F} \rangle$ is obtained by integrating the Maxwell stress tensor over a closed surface S that encloses the particle[66]

$$\langle \mathbf{F} \rangle = \oint \langle \mathbf{T} \rangle \cdot \mathrm{d}\mathbf{S} \tag{14}$$

where $\langle\ \rangle$ denotes the time average, dS is the surface enclosing the particle and T the Maxwell's stress tensor given by

$$\langle \mathbf{T} \rangle = \varepsilon_0\, \varepsilon \mathbf{EE} + \mu_0 \mu \mathbf{HH} - \frac{1}{2}\left(\varepsilon_0 \varepsilon \mathbf{E}^2 + \mu_0 \mu \mathbf{H}^2\right)\mathbf{I} \tag{15}$$

Here $\mathbf{E}$ and $\mathbf{H}$ respectively denote the electric and magnetic fields, $\mathbf{I}$ is the identity matrix, and ε and μ are the permittivity and permeability of the medium, respectively. Even though there is still debate about the correct formulation of the Maxwell stress tensor inside condensed media,[91] through these equations it is possible to determine the total optical force acting on the particle inside the nanocavity by calculating the electric and magnetic fields over the closed surface enclosing the particle. The electromagnetic fields are often retrieved through finite element method (FEM) or finite-difference time-domain (FDTD) algorithms.[92–94] The corresponding trapping potential (U) of a nanoparticle located at $\mathbf{r}_{\mathrm{NP}}$ can be determined by[66,93]

$$U(\mathbf{r}_{\mathrm{NP}}) = -\int_{\infty}^{\mathbf{r}_{\mathrm{NP}}} \mathbf{F}(\mathbf{r}) \cdot \mathrm{d}\mathbf{r} \tag{16}$$

The trapping potential determines the strength and stability of the trapping and thus defines an important figure of merit for optical trapping. The strength of optical trapping is characterized by trapping stiffness (K), which is defined as the applied optical force per unit of distance and laser power. When a trapped particle tries to escape from harmonically bound potential due to the Brownian motion or any other external forces, the behavior of the restoring force is similar to the elastic contribution of the simple harmonic oscillator thus it obeys the Hooke's law. Accordingly, by calculating the position variance of trapped particle $\langle x^2 \rangle$, the trapping stiffness along the x-axis is determined as[66,70]

$$K_x = k_{\mathrm{B}} T \left\langle x^2 \right\rangle^{-1} \tag{17}$$

According to Equation (17), a high value for the optical stiffness corresponds to small fluctuations of the particle around the equilibrium point, which leads to maximum optical stability. In such stable conditions, the escape time from the trap potential depth is expected to follow the Kramers escape rate[78,79]

$$t_{\mathrm{esc}} = \tau_0\, e^{\frac{U}{k_{\mathrm{B}}T}} \tag{18}$$

The time constant τ_0 is defined as the ratio of the drag coefficient $\beta = 6\pi\mu_{\mathrm{l}}a$ (where μ_{l} is the viscosity of the surrounding liquid) divided by the trap stiffness K. Given the trapping stiffness $K = 0.01$ pN nm^{-1}, for example, it takes about $t_{\mathrm{esc}} \approx 2.2$ s for a 50 nm sized particle to escape from 10 $K_{\mathrm{B}}T$ deep potential well filled with water ($\mu_{\mathrm{l}} \approx 1$ mPa s).

Since several applications demand long trapping time to detect and manipulate the target object, potential wells with energy higher than the thermal contribution are desired. In principle, a potential well with 1 $K_{\mathrm{B}}T$ depth is sufficient to overcome the thermal energy of the particle and localize it in the optical trap.[93] However, as it was experimentally demonstrated, the threshold limit for stable trapping is around 10 $K_{\mathrm{B}}T$.[69] Saleh and Dionne theoretically demonstrated that a coaxial plasmonic aperture, composed of a dielectric ring embedded in a noble metal (**Figure 6**a), can provide dual trapping potential well with 27 $K_{\mathrm{B}}T$ depth and 46 nm width (Figure 6b). The depth of the potential well and the magnitude of the pulling optical force can be further increased by controlling the position of the trapped particle with respect to the coaxial aperture (Figure 6c,d). Since 10 $K_{\mathrm{B}}T$ depth is sufficient to trap a nanoparticle, 10 nm particle can be stably trapped in such a deep potential well with optical power below 20 mW. By tapering the thickness of the coaxial dielectric channel, they realized trapping of dielectric particles as small as 2 nm with optical power less than 100 mW.[93] Most recently, Yoo et al. experimentally demonstrated 10 nm gap coaxial plasmonic aperture with a sharp potential well, capable of trapping 30 nm polystyrene nanoparticles and streptavidin molecules with a laser power as low as 4.7 mW.[92] Concurrently, Lu et al. demonstrated that the width and depth of plasmonic potential well can be flexibly adjusted by tuning the wavelength of the incident light.[95] For a nanoparticle trapped in a bowtie-shaped plasmonic nanocavity (Figure 6e), the depth of the trapping potential depends not only on the position of the trapped particle but also on the excitation wavelength (Figure 6f). As a result of strong plasmon coupling between the nanoparticle and the cavity, potential depth as high as 16 $K_{\mathrm{B}}T$ can be achieved by trapping 55 nm gold nanoparticles with laser intensity $I = 4 \times 10^{-8}$ W m^{-2} (Figure 6g). Generally, the trapping potential is sensitively dependent on the geometry and material of the nanostructure, as well as the size, shape, and dielectric constant of the particle being trapped.[66] The summary of optical trapping configurations involving plasmonic nanocavities is provided in **Table 1**.

3.5. Challenges and Opportunities of Plasmonic Nanotweezers

Trapping metallic nanoparticles with resonant excitation leads to strong absorption and scattering of light, which increases the relative contribution of the scattering force and makes stable trapping more challenging.[96] Another issue with trapping metallic nanoparticles is the local heat generation, proportional to the field enhancement by the nanoparticles.[97] The heat generated by the metallic nanoparticles trapped in a liquid medium gives rise to bubble formation, particle migration along the temperature gradient, hence enhanced Brownian motion—all affecting the trapping stability and the overall trapping process.[98–100] To overcome these challenges, plasmonic nanoparticles have often been trapped under off-resonant condition.[96,97,101] Similarly, optical trapping through POTs of heat-sensitive specimens such as yeast cells, *Escherichia coli* bacteria, and DNA molecules needs serious caution.[102–105] Indeed, when trapping biological samples

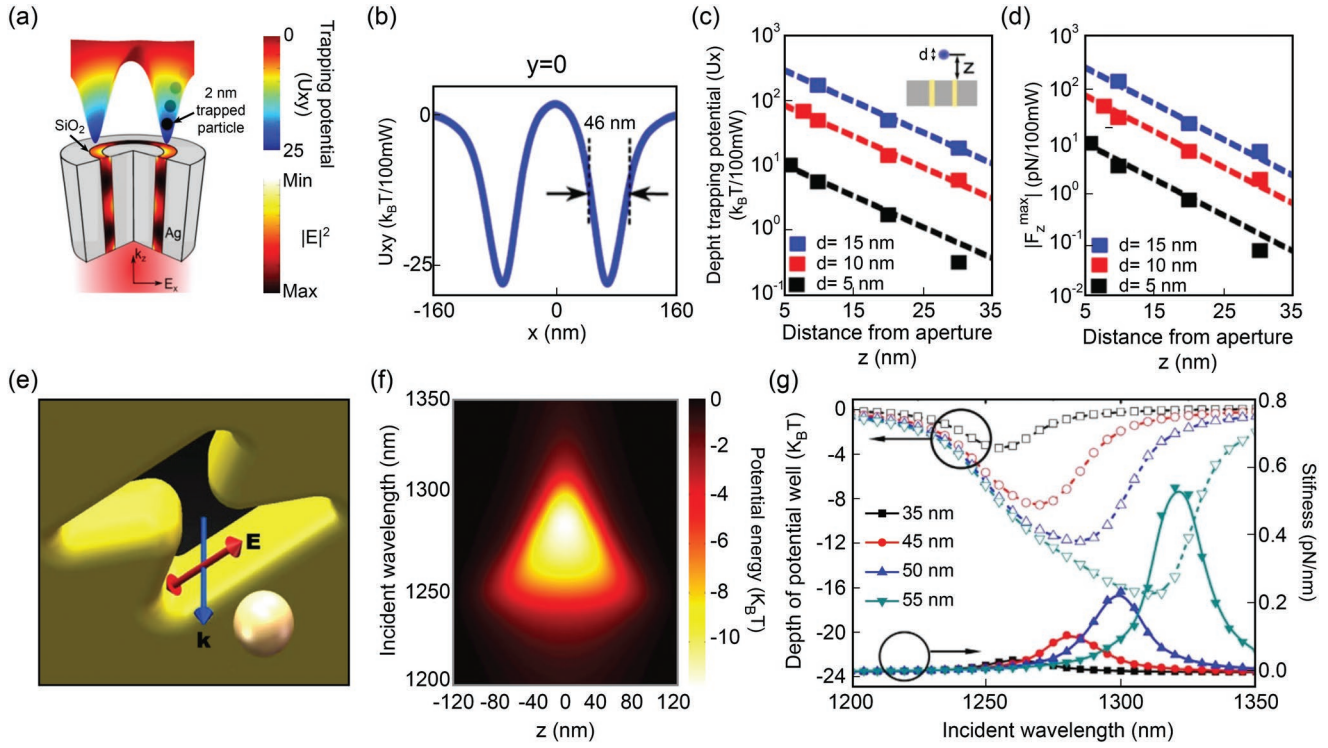

Figure 6. Trapping potentials and optical forces of plasmonic nanocavities. a) Schematic of a coaxial plasmonic nanoaperture composed of a silica ring embedded in silver slab. Sub-10 nm spherical dielectric nanoparticle with refractive index of 2 can be trapped in the dual trapping potential U_{xy} with hugely enhanced local field intensity $|\mathbf{E}|^2$. b) Cross section of the trapping potential along the *x*-axis with 27 K_BT depth and 46 nm full-width at half-maximum. c) Depth of the trapping potential as a function of the particle distance from the coaxial aperture. d) Corresponding optical force plotted for the particle diameter *d* is varied as 15, 10, and 5 nm. e) Scheme of trapping gold nanoparticles in bowtie-shaped plasmonic nanocavity. f) Corresponding trapping potential energy as a function of incident light wavelength. The potential depth reaches 12 K_BT for the indent wavelength of 1280 nm. For fixed cavity gap of 70 nm, the potential depth and trapping stiffness can be further increased by simultaneously varying the incident wavelength and nanoparticle size g). a–d) Reproduced with permission.[93] Copyright 2012, ACS Publications. e–g) Reproduced with permission.[95] Copyright 2016, Springer Nature.

by means of plasmonic nanostructures, the net optical power should not exceed the damage threshold of the specimens.[106–108]

From an application point of view, the optical heat generated by metallic nanostructures limits the possibility of integrating POTs with other kinds of opto-electronic devices.[109] The excitation of surface electrons invariably generates a large amount of heat, which in turn creates a large temperature gradient that can cause a repulsive force between the trapped particle and the hot temperature zone, thus hindering stable trapping. To turn this drawback into an advantage, new low-power optical tweezing techniques that capitalize on the photo-induced heating of plasmonic nanostructures have been devised.[110,111] Recently, Ndukaife et al. have introduced a hybrid electro-thermo-plasmonic nanotweezer that exploits the synergistic effects of an externally applied electric field and plasmonic field enhancement of gold nanoantenna, leading to long range trapping of nanoparticles.[87,112] Most recently, another novel opto-thermo-electric trapping technique that exploits plasmonic heating has been developed by Lin et al.[88] By optically heating a thermoplasmonic substrate, a light-directed thermoelectric field can be generated due to spatial separation of dissolved ions within the heating laser spot, which allows manipulation

Table 1. Main parameters of optical trapping in plasmonic nanocavities.

Configuration	Trapping cavity		Trapped particle		Trapping light	
	Gap size [nm]	Potential [K_BT]	Material	Size [nm]	Intensity [W m^{-2}]	Wavelength [nm]
Conventional Tweezer[69]	–	–	Dielectric (silica beads)	26	4.46×10^{12}	514.5
Coaxial aperture[92]	10	32	Dielectric (polystyrene)	30	4.7×10^{9}	785
Coaxial aperture[93]	25	27	Dielectric ($n = 2$)	10	20×10^{9}	692
Double nanohole aperture[94]	20	–	Dielectric (quantum dot)	8	1×10^{9}	650
Bowtie aperture[95]	70	16.5	Metallic (gold)	55	0.4×10^{9}	1310
Single nanohole aperture[106]	400	–	Biological (DNA molecule)	0.68	7.8×10^{9}	1050

of nanoparticles of a wide range of materials, sizes and shapes with single-particle resolution.[113] With simple optics, versatile low-power operation, applicability to diverse nanoparticles and tunable working wavelength, hybrid opto-thermo-electric nanotweezers are expected to become a very important tool in colloid science and nanotechnology.[88,113]

Finally, it is worth discussing recent developments in optical trapping from the aspect of nonlinear optical characterization and its implication for industrial applications. The possibility to trap and move 3D nano/microobjects is appealing for characterization of optical properties at high intensity light fields. Nonlinear optics of laser trapped matter appears as a straightforward application of laser tweezers and two-photon absorption was demonstrated under continuous wave irradiation in conventional laser tweezers.[114] However, in many practical situations, temperature increase at the laser trap affects the trapping stiffness and can lead to release of the trapped object in direct Gaussian or SIBA traps.[115] By employing nanotextured and antireflective black-Si, much higher light intensity can be applied to pin microparticles to the surface.[86] Focused laser beam pushes micro-objects to the surface where SIBA trapping facilitates pinning and binding microparticles. Due to antireflective properties of black-Si surface and high thermal conductivity of the crystalline Si, an order of magnitude higher intensity of light can be used for optical fixation of microparticles. This is expected to open possibility of characterization of nonlinear properties of microparticles and nanomaterials.

Moreover, thermally induced Marangoni flow in solution is a standard consequence when laser tweezers are used in the presence of absorption at the focal volume.[116] These thermally activated flows can be used to collect solid fractions of nano/micromaterials at the laser focus where trapping is taking place while hot solution is fueling the thermal circulation. As the laser trapped material is collected and aggregated at the focus, strong changes in laser trapping conditions can be observed. High intensity of light can also induce optical reordering at the focus as shown in the case of liquid crystals[117] and phase transitions in gels.[118] An interesting situation occurs when bubbles are formed inside the liquid phase. Shape changes induced by linear momentum of light induces dimples on the surface of bubbles and facilitates trapping of an object similar to the SIBA principle.[119] This principle of laser pinning of a bubble was implemented to remove them from a glass melt. Bubbles become unstable and undergo shape change and pinning followed by disintegration. This method was developed aiming a bubble removal in large-scale glass manufacturing.

4. Optical Trapping-Induced Resonance Shift of Plasmonic Nanocavities

The resonance wavelength of a resonant cavity is highly sensitive to its dielectric environment so that a small modification of its optical near-field, for example, by optical trapping of nanoparticles or adsorption of small molecules in the cavity region causes resonance peak shift.[120–123] A general expression of the relationship between the sensitivity of the cavity with material properties, geometrical parameters, as well as dielectric environment is, therefore, very important for understanding, analyzing, and developing trapping-assisted biosensors.[14] To this end, explicit analytical expressions that accurately predict a nano-object trapping-induced resonance perturbation have been derived for various micro/nanocavities.[14,120] Here, we discuss the physical principles behind the resonance frequency shift of plasmonic nanocavities upon trapping of a single nanoparticle or adsorption of small molecules both from sensing and optical trapping contexts.

4.1. Trapping-Induced Resonance Shift

For quantitative expression of trapping-induced resonance shift $\Delta\omega_i$ of resonant cavities (**Figure 7**), is mostly adopted the model from dielectric microcavity systems, in which the resonance shift can be expressed as the shift of the cavity eigenmode i[14]

$$\Delta\omega_i = \frac{-\omega_i}{2}\frac{\int \Delta\varepsilon(\mathbf{r})|\mathbf{E}(\mathbf{r})|^2\,\mathrm{d}\mathbf{r}}{\int \varepsilon(\mathbf{r})|\mathbf{E}(\mathbf{r})|^2\,\mathrm{d}\mathbf{r}} \tag{19}$$

Equation (19) shows a linear relationship between the resonance frequency shift and the local field intensity. However, this expression is only applicable to nanocavities made of nonlossy materials. For nanostructures made of dissipative materials, such as plasmonic nanocavities, the denominator $\int \varepsilon(\mathbf{r})|\mathbf{E}(\mathbf{r})|^2\,\mathrm{d}\mathbf{r}$ in Equation (19) vanishes, leading to unphysically large value of resonance frequency shift. Moreover, Equation (19) does not model the back-action of trapped nanoparticles.

In order to include also the back action from the nanoparticle, Zhang and Martin derived a simple but general expression capable of predicting the resonance frequency shift of subwavelength plasmonic nanocavities interacting with a nanoparticle located in the near-field zone of the nanocavity itself.[14] Such perturbation causes resonance frequency shift of the nanocavity due to near-field coupling. Using perturbation theory[120] and Green's tensor technique, the authors derived a general expression for nanoparticle trapping-induced resonance frequency shift of plasmonic nanocavity as

$$\Delta\omega_i = -\alpha_{\mathrm{NP}}\frac{\mathrm{d}\omega_i}{\mathrm{d}\varepsilon_{\mathrm{ca}}}\frac{|\mathbf{E}(\mathbf{r}_{\mathrm{NP}})|^2}{\int_{\mathrm{cavity}}|\mathbf{E}(\mathbf{r})|^2\,\mathrm{d}\mathbf{r}} \tag{20}$$

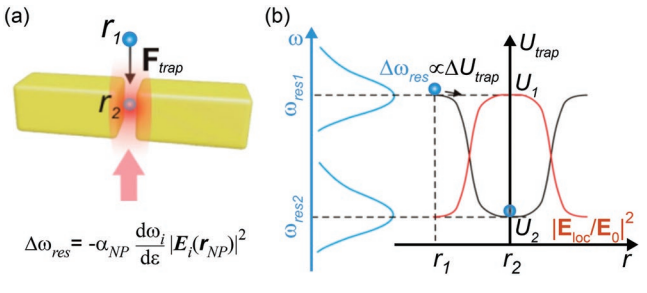

Figure 7. a) Schematic representation of nanoparticle trapping in plasmonic nanocavity. b) Optical trapping-induced cavity resonance shift (blue curve) and energy change (right). Reproduced with permission.[14] Copyright 2014, ACS Publications.

where α_{NP} is the polarizability of the nanoparticle, ε_{ca} permittivity of the nanocavity, and r_{NP} is the location of the trapped nanoparticle or adsorbed molecule. Equation (20) provides a general expression for trapping-induced resonance frequency shift of subwavelength nanocavities. This expression is universal so that it is applicable to any type of nanocavity, irrespective of size, shape, and material composition.[14] Accordingly, it provides the general guidelines for designing ultrasensitive plasmonic nanosensors since the sensitivity of nanocavity is determined by two important factors: the material dispersion $d\omega_i/d\varepsilon_{ca}$ and the local field intensity $|E|^2$. To achieve high sensitivity, thus, one needs to design hot spots with a large local field intensity by means of plasmonic nanostructures with ultrasmall nanocavities

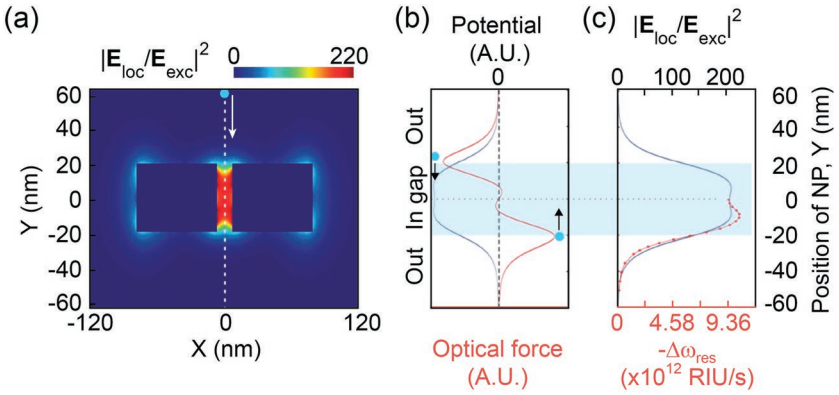

Figure 8. Relationship between optical trapping forces, trapping potential, and associated resonance frequency shifts for a gold dimer nanocavity with dimensions of 60 nm × 40 nm × 40 nm arm and 25 nm gap. a) Local field intensity map of the nanocavity. b) Optical trapping potential (blue curve) and corresponding optical force (red curve) of a 10 nm Au nanoparticle trapped along the minor axis of the nanocavity (dashed line in (a)). c) Optical trapping potential (blue curve) and trapping-induced resonance frequency shift (red curve) of the nanocavity along the dashed line in (a). Reproduced with permission.[14] Copyright 2014, ACS Publications.

4.2. Relation between Resonance Shift and Trapping Potential

From the optical trapping perspective, the resonance shift of a nanocavity upon trapping events is associated with the optical forces and overall variation of the system energy.[14] Therefore, it is important to discuss Equation (20) from the energy perspective in order to develop a relationship between the resonance shift and optical trapping potential. When a nanoparticle enters into the near field zone of plasmonic nanocavity, the nanoparticle will be polarized by the electric field. Consequently, the energy of the particle–cavity system will be changed by[14]

$$\delta U_i = \frac{-1}{2}\mathbf{P}\cdot\mathbf{E}_i(\mathbf{r}_{NP}) = \frac{-1}{2}\alpha_{NP}\left|\mathbf{E}(\mathbf{r}_{NP})\right|^2 \tag{21}$$

where $\mathbf{P}$ is the dipole moment of the trapped nanoparticle. When the polarizability α_{NP} is positive, ΔU will be negative and trapping force will be induced.[14] On the other hand, for a small particle with optical force $\mathbf{F}(\mathbf{r}_{NP}) = \frac{1}{2}\alpha_{NP}\nabla\left|\mathbf{E}(\mathbf{r}_{NP})\right|^2$, the trapping potential given in Equation (16) will be

$$U(\mathbf{r}_{NP}) = -\int_{\infty}^{r_{NP}}\mathbf{F}(\mathbf{r})\,d\mathbf{r} = \frac{1}{2}\alpha_{NP}\left|\mathbf{E}(\mathbf{r}_{NP})\right|^2 \tag{22}$$

Thus, by comparing the trapping potential given in Equation (22) with the corresponding trapping induced resonance frequency shift shown in Equation (20), it can be easily realized that both quantities are proportional to the polarizability of the trapped nanoparticle and the intensity of local field. This leads to a simple relation

$$\Delta\omega_{res} \propto U \tag{23}$$

This linear relationship between the resonance shift and the trapping potential is illustrated by the numerical simulation results provided in **Figure 8**.[14] For a 10 nm Au nanoparticle trapped in a plasmonic dimer nanocavity with 60 nm × 40 nm × 40 nm dimensions and 25 nm cavity gap, the local field is hugely enhanced and homogeneously distributed in the dimer cavity gap (Figure 8a). Based on this field distribution, the corresponding optical force and trapping potential calculated along the minor axis of the dimer cavity are shown in Figure 8b. It is worth noticing that the trapping potential depth attains its maximum value around the center of the nanocavity, where the net optical force is zero. However, as the trapped particle attempts to leave the potential well, the optical force pulls the particle to the equilibrium position (see sketch of blue circles). The nanoparticle trapping-induced resonance shift of the coupled nanosystem as a function of the location of the trapped nanoparticle ($\mathbf{r}_{NP}$) is also displayed in Figure 8c. The profiles of curves of U versus $\mathbf{r}_{NP}$ and $\Delta\omega_{res}$ versus $\mathbf{r}_{NP}$ fit each other very well. These numerical results support the linear relationship given in Equation (23).

The linear relation between the trapping potential and corresponding resonance shift has also been observed in the experimental work reported by Zhang et al.[121] They trapped 20 nm Au nanoparticles in a plasmonic dimer nanocavity with 25 nm gap (**Figure 9**). At the early stage of the trapping process, the resonance wavelength of the coupled nanosystem tends to be fixed around 690 nm, before exhibiting a sudden red shift of 50 nm at the time T_1, which indicates a trapping occurred in the cavity gap (Figure 9a,b). After instant T_2, the resonance wavelength becomes stable at 740 nm. The oscillation of the resonance wavelength between 690 and 740 nm implies that the trapped nanoparticle swings back and forth between the two states, namely, inside and outside the nanocavity. To ensure that the red shift is attributed to the optical force, additional measurements were performed with the trapping laser switched off and the results confirmed that the Rayleigh scattering returned back to its original position of 690 nm, implying that the resonance shift was caused by the perturbation of the trapped nanoparticles.[121] This fact was further confirmed by performing numerical calculations of scattering spectra of the coupled nanosystem (Figure 9c). When the Au nanoparticle is at the extremity of the antenna (cyan continuous line—end), the scattering resonance shifts only a few nanometers.

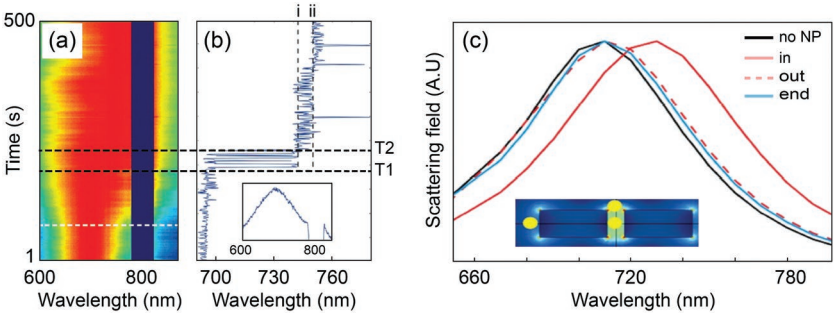

Figure 9. Nanoparticle trapping-induced scattering resonance shift. a) Plot of normalized Rayleigh scattering spectral shift induced by trapping of a 20 nm Au nanoparticle in plasmonic dimer nanocavity with 25 nm dimer gap. b). Corresponding resonance peak wavelength of the spectra as a function of time. T_1 and T_2 are trapping moments where the resonance wavelength changes its peak position. The inset represents typical Rayleigh spectra measured along the white dashed line shown in (a). c) Simulated Rayleigh scattering spectra of the same nanoantenna with 20 nm Au nanoparticles placed at different locations as shown in the inset. When the nanoparticle is placed inside the nanocavity, the scattering resonance wavelength shows significant redshift. Reproduced with permission.[121] Copyright 2010, ACS Publications.

However, when the nanoparticle is placed inside the gap of the nanocavity (red continuous line—in), the scattering spectrum shows about 20 nm red shift, which can be attributed to perturbation induced by the trapping of the nanoparticle. It is evident from the scattering spectra that, as a result of huge field enhancement in the cavity gap, trapping nanoparticles in the cavity region produces a significantly larger red shift than their trapping at the extremities of the nanocavity, which further supports the linear relationship between resonance shift and local field intensity given in Equation (17).

5. Biosensing with Plasmonic Nanoaperture Tweezers

The theoretical discussions presented under Section 4 imply that the principles of optical trapping and sensing can be merged together using plasmonic nanocavities. The traditional sensing methods require binding molecules to the ad-hoc functionalized surfaces, thus avoiding the practical recyclability of the device, unless additional processes are introduced to regenerate the surface.[122] To overcome these challenges, nano-aperture optical tweezers have emerged as an alternative approach for the detection and identification of biological molecules and their interactions at the single entity level.[123] Compared with other single molecule detection approaches, biosensing with nano-optical tweezers offers intrinsic information about the trapped objects with label-free, free-solution, low cost, and scalable operation. To advance these developments, plasmonic nanocavities with huge local field intensities and high transmission efficiency have emerged as the most promising architectures. Particularly, in the last few years, DNH apertures in gold film have been extensively used to trap and sense biomolecules and dielectric nanoparticles.[46] Using the double nanohole optical tweezer integrated with the conventional inverted microscope laser-trapping system (**Figure 10**a), Gordon group have successfully demonstrated the detection and identification of biological molecules and their interactions.[25,26,29,43–46,123–127]

They also quantified the trapping efficiency of the DNH apertures by measuring their trapping stiffness using autocorrelation analysis of Brownian fluctuations and trapping transient analysis.[124] Both of the methods yielded a consistent stiffness value of ≈0.2 fN nm^{-1} for 2 mW of laser power, which gives the stiffness per unit power efficiency of about 0.1 (fN nm^{-1}) mW^{-1}.[127] Moreover, the mean optical trapping time of the DNH aperture tweezers shows a linear relationship with the size and concentration of the trapped nanoparticles.[29]

By employing the double nanohole optical tweezer, Pang and Gordon experimentally demonstrated the trapping and unfolding of a single bovine serum albumin (BSA) molecule with a radius of 3.4 nm.[125] The unfolding of the BSA was confirmed by experiments with various optical powers and changing solution concentration. Similarly, by measuring the optical transmission through the DNH aperture, Balushi et al. experimentally demonstrated trapping of 20 nm biotin-coated PS particle and its binding with streptavidin molecule.[126] The biotin–streptavidin binding had been detected by an increase in the optical transmission through the DNH (Figure 10b). To assure that the observed increase in optical transmission was due to the specific binding of streptavidin to biotin, they also performed two control experiments using saturated streptavidin and nonfunctionalized PS particles, with neither of them resulting in a similar optical transmission behavior. By adopting the same trapping system, Kotnala and Gordon studied the interaction between p53 protein and DNA-hairpins.[43] They demonstrated the unzipping of individual 10 base pair DNA-hairpins, and quantified how tumor suppressor p53 protein could delay the unzipping (Figure 10c). This long unzipping delay (≈10 s) implies a strong binding between the p53 protein and DNA molecule (Figure 10c inset (i)). The cumulative probability shown in Figure 10c inset (ii) reveals that, for a given probability range, the unzipping time (Δt) is always greater than 1 s for wild type of p53-DNA complex as compared to DNA only. The energy barrier to the unzipping suppression (see Figure 10c inset (iii)) is found to be about $\Delta U = 2 \times 10^{-20}$ J, which is lower than the binding energy of p53 ($\Delta G = 6.9 \times 10^{-20}$ J). Further details on the biosensing with nanoaperture optical tweezers can be found from recent reviews by Gordon and co-workers.[123,127]

5.1. Raman Spectroscopy of Optically Trapped Nanoparticles

While the aforementioned results unveil the potentials of plasmonic nanocavities for trapping and sensing of single nanoparticles and small molecules, it has also been of considerable interest to identify the spectroscopic fingerprints of the trapped molecules and particles.[29,128–131] To meet this demand, nanoaperture POTs have been combined with Raman spectroscopy.[132,133] Kerman et al. experimentally demonstrated the detection and identification of single dielectric nanoparticles

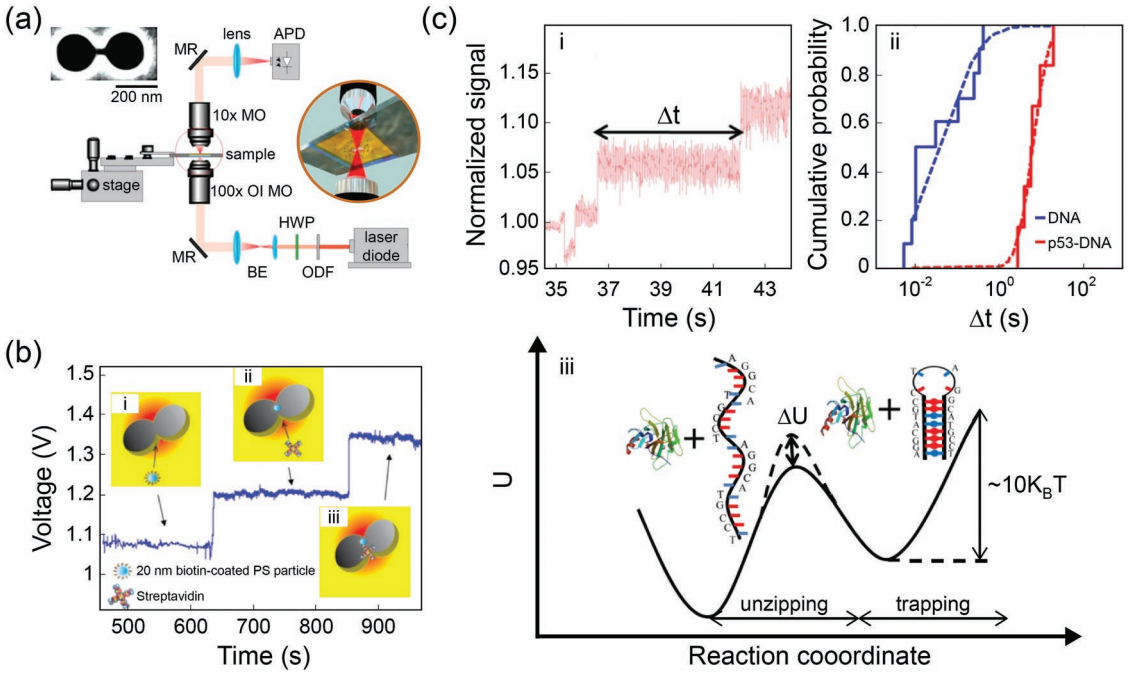

Figure 10. Biosensing with plasmonic double nanohole (DNH) aperture tweezers. a) Schematic of the DNH optical trapping system. Abbreviations: ODF = optical density filter; HWP = half wave plate; BE = beam expander; MR: mirror; OIMO: oil immersion microscope objective; APD = avalanche photodiode. The rectangular inset is a scanning electron microscope (SEM) image of the DNH fabricated using a focused ion beam (FIB). The circular inset shows a gold DNH with 20 nm polystyrene spheres suspended in water. Reproduced with permission.[126] Copyright 2013, OSA Publishing. b) Time trace of optical transmission through the DNH where i): flowing 20 nm biotin-coated polystyrene (PS) particles through the microfluidic channel, ii): trapping of 20 nm biotin-coated PS particle between the two sharp tips formed by two overlapping DNHs and subsequently flowing streptavidin, and iii): binding between 20 nm biotin-coated PS particle and streptavidin. Reproduced with permission.[126] Copyright 2013, OSA Publishing. c) Suppression of DNA hairpin unzipping by tumor suppressor protein p53. i) The wild type p53 suppresses the unzipping of the DNA hairpin for a delay of about 10 s. ii) Comparison of cumulative probability of unzipping time Δt for p53-DNA complex and DNA alone. iii) Energy reaction diagram showing increased energy barrier ΔU which is comparable with the binding energy ΔG of p53 and DNA. Reproduced with permission.[43] Copyright 2014, OSA Publishing.

trapped in plasmonic nanopores. Raman tweezers comprised of gold coated plasmonic nanopores with intensely confined local fields are capable of trapping and identifying a 20 nm polystyrene nanoparticles with a single SERS peak at 785 cm^{-1} (**Figure 11**a). Similarly, by combining surface enhanced Raman spectroscopy with nanohole optical tweezers, Jones et al. demonstrated trapping of single 20 nm titania nanoparticles and simultaneously recorded their Raman spectra.[29] For the trapped state with enhanced transmission (see Figure 11b), the Raman spectrum shows a Stokes peaks at 145, 399, 516, and 640 cm^{-1} (Figure 11c). These results imply that optical trapping assisted Raman spectroscopy, which takes the advantages of nanoparticle manipulation with unique identification, may be useful to investigate the characteristics of small molecules such as DNA and viruses at the single molecule level.

5.2. Optical Trapping-Assisted SERS Biosensors

The increasing interested in exploiting the dual potentials of Raman tweezers to trap and detect nanoparticles simultaneously, and to extend the label-free sensing and detection to the single-molecule level has been demonstrated by a number of recent works.[134–137] In this regard, Yuan et al. have presented an in-depth review of advancements in optical trapping-assisted SERS biosensing platforms.[137] The conventional optical trapping-assisted SERS sensor is comprised of far-field optical trapping components and SERS detection module (**Figure 12**a). The optical trapping system is used to trap the target objects whereas the SERS module collects the fingerprint signals of the analytes adsorbed on the nanoaggregates. Under high power excitation, the Raman signals of analytes adsorbed by the target objects (usually metallic nanoparticles or nanoaggregates) can be extracted. However, the far-field optical trapping-assisted SERS sensing is diffraction limited and employs high laser power, which make it not preferable to detect and sense nanosized biological specimens that are prone to photo-induced damage. To overcome these challenges, near-field optical trapping-assisted SERS sensors, which capitalize on the local field intensity of plasmonic nanostructures, have been devised for biosensing applications.[137] Furthermore, unlike far-field optical trapping schemes, the near-field optical trapping Raman sensors do not require high laser power and high NA. As shown in Figure 12b, such platforms are made of plasmonic nanostructures integrated with conventional optical trapping components and SERS sensing elements. For the realization of plasmonic Raman tweezers, metallic nanocavities with high local field intensity would be the ideal candidates. By utilizing thermal sensitivity of Raman active modes as demonstrated for the SiGe nanoparticles,[138]

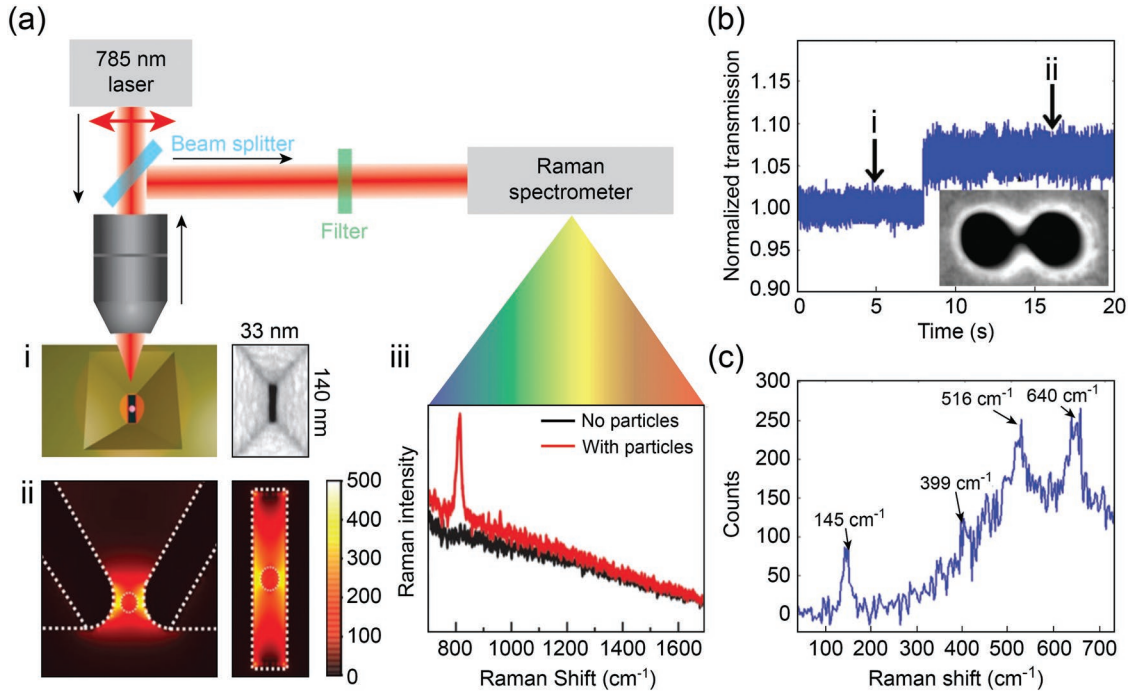

Figure 11. Raman Spectroscopy of optically trapped single nanoparticles. a) Schematics of experimental setup of Raman tweezer comprising a 785 nm laser, beam splitter, 60× (NA 0.9) water immersion objective, long-pass filter, Raman spectrometer. i) 3D representation (left) and SEM image (right) of the gold coated nanopore. ii) FDTD simulation intensity profile of the nanopore from the side (left) and from the top (right). iii) Raman spectra with and without a 20 nm carboxyl modified polystyrene particle inside the nanopore. Reproduced with permission.[133] Copyright 2015, OSA Publishing. b) Optical transmission of 20 nm titania nanoparticle trapped in a double-nanohole optical tweezer system shown inset. The arrows show nontrapping i) and trapping ii) states of the nanoparticles. c) The characteristic Raman spectrum of the nanoparticle in its trapped state. Reproduced with permission.[26] Copyright 2015, The Royal Society of Chemistry.

such plasmonic Raman tweezers can have an additional virtue to read local temperature at the nanoscale.

6. Concluding Remarks

We have discussed the fundamental mechanisms and peculiarities of plasmonic nanocavities for optical trapping and detection of single nanoparticles and small molecules. The optical responses of plasmonic nanocavities strongly depend on the design and intrinsic properties of the nanocavities.[59,60] The plasmonic enhancement of nanocavities can be safely described by pure classical electromagnetic theory for nanocavities with single-digit-nanometer gaps. However, when the cavity size enters sub-nanometer regime, the quantum mechanical effects such as nonlocal screening and electron tunneling emerge, with a consequent reduction of the local field enhancement.[34,35] Such ultimate limitations of plasmonic enhancements in ultrasmall nanocavities can be tackled by using nanocavities with fixed gap sizes but extra field confinement abilities. For example, split-ring dimer nanocavities have proved to confine the electromagnetic field both in the dimer and split gaps with remarkable intensities.[139–141]

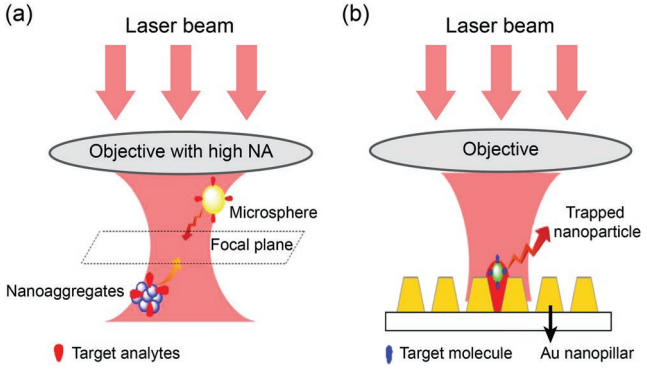

Figure 12. Schematic illustrations of SERS biosensing platforms based on a) conventional optical trapping and b) plasmonic optical trapping. Reproduced with permission.[137] Copyright 2017, Elsevier.

Properly designed plasmonic nanocavities can provide strongly enhanced local fields and deep trapping potential, implying their capability for trapping nanosized objects with low laser power. Thus, we have also discussed about the theoretical basis and experimental demonstrations of optical trapping of nanosized objects in plasmonic nanocavities. The active role of trapped nanoparticles via self-induced back-action effect further enhances the local field intensity of the system and hence leads to trapping with minimum optical power. The local heating problem associated with plasmonic nanostructures can be turned into advantage by using the heat for devising thermoplasmonic nanotweezers. We have also discussed about analytical expressions describing the relationship between resonance shift and potential energy of the trapping systems. It has been demonstrated that the optical trapping-induced resonance

shift and the trapping potential can be expressed in terms of the local field intensity of the nanocavity. For further information on the current developments of plasmonic nanotweezers and their applications, interesting works have been recently published.[127,135,142,143]

Apart from the theoretical analysis, we have also discussed recent experimental demonstrations of optical trapping-assisted biosensing employing plasmonic nanoapertures. Particularly, recent reports merging together plasmonic optical tweezers and Raman spectroscopy for the identification of the fingerprints of optically trapped nanoparticles and small molecules have been covered. These works have led to the proposal of an ambitious sensing platform that can simultaneously perform single-molecule trapping and detection. To meet this demand, an optical trapping-assisted Raman biosensor that takes the advantage of nanoparticle manipulation ability of plasmonic optical tweezers and particle detection potential of Raman spectroscopy has been proposed. We suggest that, to realize such a novel biosensing device, plasmonic nanohole apertures will play a key role.

Acknowledgements

T.W. thanks the National Natural Science Foundation of China (Grant No. 61804036), and the Zhejiang Province Commonweal Project (Grant No. LGJ20A040001). J.C. acknowledges CAS-TWAS President's Fellowship funding. R.P.Z. would like to recognize the support from 3315 project (project number Y70001DL01) of Ningbo/Cixi, Zhejiang province, China.

Conflict of Interest

The authors declare no conflict of interest.

Keywords

nanocavities, optical tweezers, plasmonics, trapping

Received: September 2, 2019
Revised: December 18, 2019
Published online: February 27, 2020

[1] L. Novotny, B. Hecht, *Principles of Nano-Optics*, Cambridge University Press, New York, USA **2012**.
[2] U. Hohenester, *Nano and Quantum Optics: An Introduction to Basic Principles and Theory*, Springer, Cham, Switzerland **2020**.
[3] J. Weiner, F. Nunes, *Light-Matter Interaction: Physics and Engineering at the Nanoscale*, Oxford University Press, Oxford, UK **2017**.
[4] K. Das, B. Hazra, M. Chandra, *Phys. Chem. Chem. Phys.* **2017**, *19*, 27997.
[5] L. Neumeier, R. Quidant, D. E. Chang, *New J. Phys.* **2015**, *17*, 123008.
[6] A. A. Lyamkina, K. Schraml, A. Regler, M. Schalk, A. K. Bakarov, A. I. Toropov, S. P. Moshchenko, M. Kaniber, *Opt. Express* **2016**, *24*, 28936.
[7] A. B. Taylor, P. Zijlstra, *ACS Sens.* **2017**, *2*, 1103.
[8] M. Chirumamilla, A. Gopalakrishnan, A. Toma, R. P. Zaccaria, R. Krahne, *Nanotechnology* **2014**, *25*, 235303.
[9] Z. Wang, Z. Dong, Y. Gu, Y.-H. Chang, L. Zhang, L.-J. Li, W. Zhao, G. Eda, W. Zhang, G. Grinblat, S. A. Maier, J. K. W. Yang, C.-W. Qiu, A. T. S. Wee, *Nat. Commun.* **2016**, *7*, 11283.
[10] P. Genevet, J.-P. Tetienne, R. Blanchard, M. A. Kats, J. P. B. Müller, M. O. Scully, F. Capasso, *Appl. Opt.* **2011**, *50*, G56.
[11] M. L. Juan, M. Righini, R. Quidant, *Nat. Photonics* **2011**, *5*, 349.
[12] S. A. Maier, *Plasmonics: Fundamentals and Applications*, Springer, New York **2007**.
[13] S.-Y. Ding, J. Yi, J.-F. Li, B. Ren, D.-Y. Wu, R. Panneerselvam, Z.-Q. Tian, *Nat. Rev. Mater.* **2016**, *1*, 16021.
[14] W. Zhang, O. J. F. Martin, *ACS Photonics* **2015**, *2*, 144.
[15] S. Huang, T. Ming, Y. Lin, X. Ling, Q. Ruan, T. Palacios, J. Wang, M. Dresselhaus, J. Kong, *Small* **2016**, *12*, 5190.
[16] V. Devaraj, J.-M. Lee, J.-W. Oh, *Nanomaterials* **2018**, *8*, 582.
[17] R. Chikkaraddy, X. Zheng, F. Benz, L. J. Brooks, B. de Nijs, C. Carnegie, M.-E. Kleemann, J. Mertens, R. W. Bowman, G. A. E. Vandenbosch, V. V. Moshchalkov, J. J. Baumberg, *ACS Photonics* **2017**, *4*, 469.
[18] F. Benz, C. Tserkezis, L. O. Herrmann, B. de Nijs, A. Sanders, D. O. Sigle, L. Pukenas, S. D. Evans, J. Aizpurua, J. J. Baumberg, *Nano Lett.* **2015**, *15*, 669.
[19] B. de Nijs, R. W. Bowman, L. O. Herrmann, F. Benz, S. J. Barrow, J. Mertens, D. O. Sigle, R. Chikkaraddy, A. Eiden, A. Ferrari, O. A. Scherman, J. J. Baumberg, *Faraday Discuss.* **2015**, *178*, 185.
[20] A. Kinkhabwala, Z. Yu, S. Fan, Y, A , K. Müllen, W. E. Moerner, *Nat. Photonics* **2009**, *3*, 654.
[21] M.-K. Kim, H. Sim, S. J. Yoon, S.-H. Gong, C. W. Ahn, Y.-H. Cho, Y.-H. Lee, *Nano Lett.* **2015**, *15*, 4102.
[22] I.-C. Huang, J. Holzgrafe, R. A. Jensen, J. T. Choy, M. G. Bawendi, M. Lončar, *Appl. Phys. Lett.* **2016**, *109*, 133105.
[23] H. Wang, H.-Y. Wang, A. Bozzola, A. Toma, S. Panaro, W. Raja, A. Alabastri, L. Wang, Q.-D. Chen, H.-L. Xu, F. De Angelis, H.-B. Sun, R. P. Zaccaria, *Adv. Funct. Mater.* **2016**, *26*, 6198.
[24] C. Chen, M. L. Juan, Y. Li, G. Maes, G. Borghs, P. V. Dorpe, R. Quidant, *Nano Lett.* **2012**, *12*, 125.
[25] Y. Pang, R. Gordon, *Nano Lett.* **2011**, *11*, 3763.
[26] S. Jones, A. A. A. Balushi, R. Gordon, *J. Opt.* **2015**, *17*, 102001.
[27] J. Berthelot, S. S. Aćimović, M. L. Juan, M. P. Kreuzer, J. Renger, R. Quidant, *Nat. Nanotechnol.* **2014**, *9*, 295.
[28] R. A. Jensen, I.-C. Huang, O. Chen, J. T. Choy, T. S. Bischof, M. Lončar, M. G. Bawendi, *ACS Photonics* **2016**, *3*, 423.
[29] A. Kotnala, D. DePaoli, R. Gordon, *Lab Chip* **2013**, *13*, 4142.
[30] L. Li, T. Hutter, U. Steinerc, S. Mahajan, *Analyst* **2013**, *138*, 4574.
[31] H. Wang, A. Toma, H.-Y. Wang, A. Bozzola, E. Miele, A. Haddadpour, G. Veronis, F. De Angelis, L. Wang, Q.-D. Chen, H.-L. Xu, H.-B. Sun, R. P. Zaccaria, *Nanoscale* **2016**, *8*, 13445.
[32] H. Wang, H.-Y. Wang, Q.-D. Chen, H.-L. Xu, H.-B. Sun, F. Huang, W. Raja, A. Toma, R. P. Zaccaria, *Laser Photonics Rev.* **2018**, *12*, 1700176.
[33] H. Wang, H.-Y. Wang, H.-B. Sun, A. Cerea, A. Toma, F. De Angelis, X. Jin, L. Razzari, D. Cojoc, D. Catone, F. Huang, R. P. Zaccaria, *Adv. Funct. Mater.* **2018**, *28*, 1801761.
[34] J. M. McMahon, S. Li, L. K. Ausman, G. C. Schatz, *J. Phys. Chem. C* **2012**, *116*, 1627.
[35] W. Zhu, R. Esteban, A. G. Borisov, J. J. Baumberg, P. Nordlander, H. J. Lezec, J. Aizpurua, K. B. Crozier, *Nat. Commun.* **2016**, *7*, 11495.
[36] L. Ding, J. Qin, S. Guo, T. Liu, E. Kinzel, L. Wang, *Sci. Rep.* **2016**, *6*, 27254.
[37] D. Y. Lei, A. I. Fernández-Dominguez, Y. Sonnefraud, K. Appavoo, R. F. Haglund Jr., J. B. Pendry, S. A. Maier, *ACS Nano* **2012**, *6*, 1380.
[38] Y. Huang, Q. Zhou, M. Hou, L. Ma, Z. Zhang, *Phys. Chem. Chem. Phys.* **2015**, *17*, 29293.
[39] A. N. Koya, B. Ji, Z. Hao, J. Lin, *J. Appl. Phys.* **2015**, *118*, 113101.
[40] A. N. Koya, J. Lin, *J. Appl. Phys.* **2016**, *120*, 093105.

[41] A. N. Koya, J. Lin, *Appl. Phys. Rev.* **2017**, *4*, 021104.
[42] S. Zou, G. C. Schatz, *Chem. Phys. Lett.* **2005**, *403*, 62.
[43] A. Kotnala, R. Gordon, *Biomed. Opt. Express* **2014**, *5*, 1886.
[44] R. Regmi, A. A. Al Balushi, H. Rigneault, R. Gordon, J. Wenger, *Sci. Rep.* **2015**, *5*, 15852.
[45] Y. Chen, A. Kotnala, L. Yu, J. Zhang, R. Gordon, *Opt. Express* **2015**, *23*, 30227.
[46] M. Ghorbanzadeh, S. Jones, M. K. Moravvej-Farshi, R. Gordon, *ACS Photonics* **2017**, *4*, 1108.
[47] P. T. Kristensen, C. Van Vlack, S. Hughes, *Opt. Lett.* **2012**, *37*, 1649.
[48] P. T. Kristensen, S. Hughes, *ACS Photonics* **2014**, *1*, 2.
[49] Y. Li, D. Li, C. Chi, B. Huang, *J. Phys. Chem. C* **2017**, *121*, 16481.
[50] S. A. Maier, *Opt. Quantum Electron.* **2006**, *38*, 257.
[51] S. A. Maier, *Opt. Express* **2006**, *14*, 1957.
[52] Y. Sonnefraud, N. Verellen, H. Sobhani, G. A.E. Vandenbosch, V. V. Moshchalkov, P. Van Dorpe, P. Nordlander, S. A. Maier, *ACS Nano* **2010**, *4*, 1664.
[53] D. Conteduca, C. Reardon, M. G. Scullion, F. Dell'Olio, M. N. Armenise, T. F. Krauss, C. Ciminell, *APL Photonics* **2017**, *2*, 086101.
[54] J. Zhang, J. Li, S. Tang, Y. Fang, J. Wang, G. Huang, R. Liu, L. Zheng, X. Cui, Y. Mei, *Sci. Rep.* **2015**, *5*, 15012.
[55] H. Wang, H.-Y. Wang, A. Toma, T.-A. Yano, Q.-D. Chen, H.-L. Xu, H.-B. Sun, R. P. Zaccaria, *J. Phys. Chem. Lett.* **2016**, *7*, 4648.
[56] Z.-J.N. Yang, T. J. Antosiewicz, T. Shegai, *Opt. Express* **2016**, *24*, 20373.
[57] C. Ciminelli, D. Conteduca, F. Dell'Olio, M. N. Armenise, *IEEE Photonics J.* **2014**, *6*, 0600916.
[58] S. V. Boriskina, T. A. Cooper, L. Zeng, G. Ni, J. K. Tong, Y. Tsurimaki, Y. Huang, L. Meroueh, G. Mahan, G Chen, *Adv. Opt. Photonics* **2017**, *9*, 775.
[59] R. Gordon, A. Ahmed, *ACS Photonics* **2018**, *5*, 4222.
[60] C. Ciracì, R. T. Hill, J. J. Mock, Y. Urzhumov, A. I. Fernández-Domínguez, S. A. Maier, J. B. Pendry, A. Chilkoti, D. R. Smith, *Science* **2012**, *337*, 1072.
[61] T. V. Teperik, P. Nordlander, J. Aizpurua, A. G. Borisov, *Phys. Rev. Lett.* **2013**, *110*, 263901.
[62] G. Hajisalem, Q. Min, R. Gelfand, R Gordon, *Opt. Express* **2014**, *22*, 9604.
[63] D. Doyle, N. Charipar, C. Argyropoulos, S. A. Trammell, R. Nita, J. Naciri, A. Piqué, J. B. Herzog, J. Fontana, *ACS Photonics* **2018**, *5*, 1012.
[64] A. Ashkin, *Phys. Rev. Lett.* **1970**, *24*, 156.
[65] D. G. Grier, *Nature* **2003**, *424*, 810.
[66] L. Novotny, R. X. Bian, X. S. Xie, *Phys. Rev. Lett.* **1997**, *79*, 645.
[67] S. Kawata, Y. Inouye, P. Verma, *Nat. Photonics* **2009**, *3*, 388.
[68] T. A. Nieminen, G. Knoner, N. R. Heckenberg, H. Rubinsztein-Dunlop, *Methods Cell Biol.* **2007**, *82*, 207.
[69] A. Ashkin, J. M. Dziedzic, J. E. Bjorkholm, S Chu, *Opt. Lett.* **1986**, *11*, 288.
[70] D. Conteduca, F. Dell'Olio, T. F. Krauss, C. Ciminelli, *Appl. Spectrosc.* **2017**, *71*, 367.
[71] T. Shoji, Y. Tsuboi, *J. Phys. Chem. Lett.* **2014**, *5*, 2957.
[72] L. Bosanac, T. Aabo, P. M. Bendix, L. B. Oddershede, *Nano Lett.* **2008**, *8*, 1486.
[73] O. M. Maragò, P. H. Jones, P. G. Gucciardi1, G. Volpe, A. C. Ferrari, *Nat. Nanotechnol.* **2013**, *8*, 807.
[74] A. Ashkin, J. M. Dziedzic, P. W. Smith, *Opt. Lett.* **1982**, *7*, 276.
[75] V. Garbin, D. Cojoc, E. Ferrari, E. Di Fabrizio, M. L. J. Overvelde, S. M. van der Meer, N. de Jong, D. Lohse, M. Versluis, *Appl. Phys. Lett.* **2007**, *90*, 114103.
[76] D. Cojoc, V. Emiliani, E. Ferrari, R. Malureanu, S. Cabrini, R. Z. Proietti, E. Di Fabrizio, *Jpn. J. Appl. Phys.* **2004**, *43*, 3910.
[77] P. W. Smith, P. J. Maloney, A. Ashkin, *Opt. Lett.* **1982**, *7*, 347.
[78] K. Svoboda, S. M. Block, *Opt. Lett.* **1994**, *19*, 930.
[79] M. Pelton, M. Liu, H. Y. Kim, G. Smith, P. Guyot-Sionnest, N. F. Scherer, *Opt. Lett.* **2006**, *31*, 2075.
[80] P. Mestres, J. Berthelot, S. S Aćimović, R. Quidant, *Light: Sci. Appl.* **2016**, *5*, 16092.
[81] A. Ashkin, J. M. Dziedzic, *Science* **1987**, *235*, 1517.
[82] O. J. F. Martin, C. Girard, *Appl. Phys. Lett.* **1997**, *70*, 705.
[83] K. Okamoto, S. Kawata, *Phys. Rev. Lett.* **1999**, *83*, 4534.
[84] M. Righini, A. S. Zelenina, C. Girard, R. Quidant, *Nat. Phys.* **2007**, *3*, 477.
[85] M. Righini, G. Volpe, C. Girard, D. Petrov, R. Quidant, *Phys. Rev. Lett.* **2008**, *100*, 183604.
[86] T. Shoji, A. Mototsuji, A. Balčytis, D. Linklater, S. Juodkazis, Y. Tsuboi, *Sci. Rep.* **2017**, *7*, 12298.
[87] J. C. Ndukaife, A. V. Kildishev, A. G. A. Nnanna, V. M. Shalaev, S. T. Wereley, A. Boltasseva, *Nat. Nanotechnol.* **2016**, *11*, 53.
[88] L. Lin, M. Wang, X. Peng, E. N. Lissek, Z. Mao, L. Scarabelli, E. Adkins, S. Coskun, H. E. Unalan, B. A. Korgel, L. M. Liz-Marzán, E.-L. Florin, Y. Zheng, *Nat. Photonics* **2018**, *12*, 195.
[89] M. L. Juan, R. Gordon, Y. Pang, F. Eftekhari, R. Quidant, *Nat. Phys.* **2009**, *5*, 915.
[90] P. Padhy, M. A. Zaman, P. Hansen, L. Hesselink, *Opt. Express* **2017**, *25*, 26198.
[91] M. Liu, K. Stierstadt, arXiv:cond-mat/0010261, **2000**.
[92] D. Yoo, K. L. Gurunatha, H.-K. Choi, D. A. Mohr, C. T. Ertsgaard, R. Gordon, S.-H. Oh, *Nano Lett.* **2018**, *18*, 3637.
[93] A. A. E. Saleh, J. A. Dionne, *Nano Lett.* **2012**, *12*, 5581.
[94] P. Zhang, G. Song, L. Yu, *Photonics Res.* **2018**, *6*, 182.
[95] Y Lu, G. Du, F. Chen, Q. Yang, H. Bian, J. Yong, X. Hou, *Sci. Rep.* **2016**, *6*, 32675.
[96] A. S. Urban, S. Carretero-Palacios, A. A. Lutich, T. Lohmuller, J. Feldmann, F. Jackel, *Nanoscale* **2014**, *6*, 4458.
[97] M. Dienerowitz, M. Mazilu, K. Dholakia, *J. Nanophotonics* **2008**, *2*, 021875.
[98] J. C. Ndukaife, A. Mishra, U. Guler, A. G. A. Nnanna, S. T. Wereley, A. Boltasseva, *ACS Nano* **2014**, *8*, 9035.
[99] D. W. Berry, N. R. Heckenberg, H. Rubinszteindunlop, *J. Mod. Opt.* **2000**, *47*, 1575.
[100] K. Wang, E. Schonbrun, P. Steinvurzel, K. B. Crozier, *Nat. Commun.* **2011**, *2*, 469.
[101] Z J. Coppens, W Li, D. Greg Walker, J G. Valentine, *Nano Lett.* **2013**, *13*, 1023.
[102] X. Miao, L. Y. Lin, *IEEE J. Sel. Top. Quantum Electron.* **2007**, *13*, 1655.
[103] M. Righini, P. Ghenuche, S. Cherukulappurath, V. Myroshnychenko, F. J. García de Abajo, R. Quidant, *Nano Lett.* **2009**, *9*, 3387.
[104] B. J. Roxworthy, M. T. Johnston, F. T. Lee-Montiel, R. H. Ewoldt, P. I. Imoukhuede, K. C. Toussaint Jr., *PLoS One* **2014**, *9*, 93929.
[105] M. Belkin, S.-H. Chao, M. P. Jonsson, C. Dekker, A. Aksimentiev, *ACS Nano* **2015**, *9*, 10598.
[106] J.-D. Kim, Y.-G. Lee, *Biomed. Opt. Express* **2014**, *5*, 2471.
[107] Y. Liu, G. J. Sonek, M. W. Berns, B. J. Tromberg, *Biophys. J.* **1996**, *71*, 2158.
[108] P. Jing, J. Wu, G. W. Liu, E. G. Keeler, S. H. Pun, L. Y. Lin, *Sci. Rep.* **2016**, *6*, 19924.
[109] S. V. Boriskina, H. Ghasemi, G. Chen, *Mater. Today* **2013**, *16*, 375.
[110] J. C. Ndukaife, Y. Xuan, A. G. A. Nnanna, A. V. Kildishev, V. M. Shalaev, S. T. Wereley, A. Boltasseva, *ACS Nano* **2018**, *12*, 5376.
[111] Y. Liu, L. Lin, B. B. Rajeeva, J. W. Jarrett, X. Li, X. Peng, P. Kollipara, K. Yao, D. Akinwande, A. K. Dunn, Y. Zheng, *ACS Nano* **2018**, *12*, 10383.
[112] Y. Tsuboi, *Nat. Nanotechnol.* **2016**, *11*, 5.
[113] F. Cichos, *Nat. Photonics* **2018**, *12*, 191.
[114] N. Murazawa, S. Juodkazis, H. Misawa, K. Kamada, *Mol. Cryst. Liq. Cryst.* **2008**, *489*, 310.

[115] G. Seniutinas, L. Rosa, G. Gervinskas, E. Brasselet, S. Juodkazis, J. Beilstein, *Nanotechnology* **2013**, *4*, 534.
[116] O. A. Louchev, S. Juodkazis, N. Murazawa, S. Wada, H. Misawa, *Opt. Express* **2008**, *16*, 5673.
[117] N. Murazawa, S. Juodkazis, H. Misawa, *Opt. Express* **2006**, *14*, 2481.
[118] S. Juodkazis, N. Mukai, R. Wakaki, A. Yamaguchi, S. Matsuo, H. Misawa, *Nature* **2000**, *408*, 178.
[119] N. Murazawa, S. Juodkazis, H. Misawa, H. Wakatsuki, *Opt. Express* **2007**, *15*, 13310.
[120] R. A. Waldron, *Proc. IEEE* **1960**, *107*, 272.
[121] W. Zhang, L. Huang, C. Santschi, O. J. F. Martin, *Nano Lett.* **2010**, *10*, 1006.
[122] S. Lin, K. B. Crozier, *ACS Nano* **2013**, *7*, 1725.
[123] A. A. Al Balushi, A. Kotnala, S. Wheaton, R. M. Gelfand, Y. Rajashekara, R. Gordon, *Analyst* **2015**, *140*, 4760.
[124] A. Kotnala, R. Gordon, *Nano Lett.* **2014**, *14*, 853.
[125] Y. Pang, R. Gordon, *Nano Lett.* **2012**, *12*, 402.
[126] A. A. Al Balushi, A. Zehtabi-Oskuie, R. Gordon, *Biomed. Opt. Express* **2013**, *4*, 1504.
[127] R. Gordon, *Opt. Laser Technol.* **2019**, *109*, 328.
[128] D. V. Petrov, *J. Opt. A: Pure Appl. Opt.* **2007**, *9*, S139.
[129] S. Lin, W. Zhu, Y. Jin, K. B. Crozier, *Nano Lett.* **2013**, *13*, 559.
[130] B. Redding, M. J. Schwab, Y. Pan, *Sensors* **2015**, *15*, 19021.
[131] L. Rkiouak, M. J. Tang, J. C. J. Camp, J. McGregor, I. M. Watson, R. A. Cox, M. Kalberer, A. D. Ward, F. D. Pope, *Phys. Chem. Chem. Phys.* **2014**, *16*, 11426.
[132] Y. Zhang, J. Shen, Z. Xie, X. Dou, C. Min, T. Lei, J. Liu, S. Zhu, X. Yuan, *Nanoscale* **2017**, *9*, 10694.
[133] S. Kerman, C. Chen, Y. Li, W. V. Roy, L. Lagae, P. V. Dorpe, *Nanoscale* **2015**, *7*, 18612.
[134] J. C. Cordova, D. K. Das, H. W. Manning, M. J. Lang, *Curr. Opin. Struct. Biol.* **2014**, *28*, 142.
[135] D. Garoli, H. Yamazaki, N. Maccaferri, M. Wanunu, *Nano Lett.* **2019**, *19*, 7553.
[136] F. Sinjab, D. Awuah, G. Gibson, M. Padgett, A. M. Ghaemmaghami, I. Notingher, *Opt. Express* **2018**, *26*, 25211.
[137] Y. Yuan, Y. Lin, B. Gu, N. Panwar, S. C. Tjin, J. Song, J. Qua, K.-T. Yong, *Coord. Chem. Rev.* **2017**, *339*, 138.
[138] E. Mitsai, M. Naffouti, T. David, M. Abbarchi, L. Hassayoun, D. Storozhenko, A. Mironenko, S. Bratskaya, S. Juodkazis, S. Makarov, A. Kuchmizhak, *Nanoscale* **2019**, *11*, 11634.
[139] A. N. Koya, B. Ji, Z. Hao, J. Lin, *J. Opt.* **2016**, *18*, 055007.
[140] A. N. Koya, J. Lin, *Proc. SPIE* **2016**, *10028*, 1002803.
[141] A. N. Koya, B. Ji, Z. Hao, J. Lin, *Plasmonics* **2017**, *12*, 1693.
[142] C. Bradac, *Adv. Opt. Mater.* **2018**, *6*, 1800005.
[143] K. B. Crozier, *Light: Sci. Appl.* **2019**, *8*, 35.